Geophysical Journal International

Geophys. J. Int. (2010) **183,** 1–19 doi: 10.1111/j.1365-246X.2010.04692.x

Constraints on average Taiwan Reference Moho Discontinuity Model—receiver function analysis using BATS data

Hsiao-Lan Wang,[1] How-Wei Chen[2] and Lupei Zhu[3]

[1] *Institute of Seismology and Institute of Applied Geophysics, National Chung Cheng University, Min-Hsiung, Chia-Yi* 621, *Taiwan, ROC*
[2] *Department of Earth Sciences and Institute of Geophysics, National Central University, Chung-Li* 320, *Taiwan, ROC. E-mail: hwchen@ncu.edu.tw*
[3] *Department of Earth and Atmospheric Sciences, Saint Louis University, Saint Louis,* MI 63103, *USA*

Accepted 2010 June 6. Received 2010 June 5; in original form 2009 April 4

SUMMARY

By analysing teleseismic waveform data, we propose a large-scale Taiwan Reference Moho Discontinuity Model (TRMDM) through coherent stacking and H–κ analysis of receiver functions (RFs). Tectonic structural features are determined from accurate crustal thickness (H) and reliable Vp/Vs ratio (κ) (consequently Poisson's ratio, σ) estimations for Taiwan. The best estimated regional average Moho depth is 33.5 ± 2.9 km. Noted is a westward crustal thinning from 39 ± 3.0 km in eastern Taiwan to 30 ± 1.5 km in southeastern China. The averaged Moho depth is 23.0 ± 2.5 km in northern Taiwan and increases to 33.5 ± 2.0 km in the south. The markedly thin crust and high Vp/Vs ratio in northern Taiwan are mainly associated with backarc opening and magmatic activities. Based on H–κ estimations and associated seismicity patterns beneath Suang-Long (SSLB) and adjacent four stations, we propose two Moho reference models that exhibit distinctive crustal thickening in central Taiwan. The spatial variations of crustal thickness models show strong lateral change in the Moho topography. The thick crust in the south, thin crust in the north and transition in central Taiwan mark the different tectonic units between the subduction wedge and the collision prism onshore.

In view of the following list of constraints: thicker crust in the south than in the north; eastward crust thickening; significant Moho depth changes; clear 9–11 s subcrustal boundaries from five stations; the compelling thickening of crust and upper mantle beneath the central mountain belt; seismicity patterns with the absence of mantle earthquake in the Wadati-Benioff zone; regional geological features; the occurrence of the inland Chi-Chi earthquake; the compelling low κ at YULB (1.58 ± 0.13) that may extend to central Taiwan at SSLB (1.59 ± 0.23); relatively thick crust at YULB (39.5 ± 1.6 km) and SSLB (40.5 ± 1.3 km or 52.5 ± 1.5 km), and finally, the apparent horizontal offset between highest Yu Shan Mountain and the deepest Moho at SSLB, we are able to suggest that the initial subduction of the Eurasian Plate occurred in southern Taiwan and most likely extended to the transition zone in central Taiwan. Although the current RF study is limited by large interstation distance, our analysis provides more notable constraints than previous studies to explicitly determine the characteristic features of Moho discontinuity. This detailed approach means that rather than treating the tectonic framework as a whole heterogeneous lithospheric feature, clear Moho boundary geometry variations indicate that active orogenic processes and differential tectonic stress loading create separate and complex crustal and subcrustal-to-upper-mantle structural features caused by the arc–continent collision.

Key words: Image processing; Composition of the continental crust; Continental margins: convergent; Crustal structure; Rheology: crust and lithosphere; Asia.

1 INTRODUCTION

Taiwan is located at the juncture of an active collision–subduction system where orogenic processes and tectonic evolution occur between the Eurasian Plate (EUP) and the Philippine Sea Plate (PSP). The study area includes extensive mountain ranges and is marked by numerous inland and offshore earthquakes. Various crust-to-upper-mantle scale tectonic process models have been proposed and vigorously debated to describe Taiwan orogeny and tectonic evolution; these include the 'thin-skinned' tectonic model (Suppe

1987), the 'lithospheric collision' model (Wu *et al.* 1997) and others (Hsu & Sibuet 1995; Chemanda *et al.* 1997). Even though an unprecedented number of seismic records are available for Taiwan, data from the short-period Taiwan Seismic Network operated by the Central Weather Bureau (CWB), though well calibrated for time, are collected from stations that have relatively wide interstation spacing and are consequently limited in their capability to image small-scale shallow velocity structural features. Surface wave inversion (Hwang & Yu 2005) provides an alternative approach to estimating 1-D upper-mantle velocity structure; however, the approach does not resolve crustal properties well due to limited ray coverage owing to the predominantly horizontally propagating surface waves, short propagation distances from inland earthquake and low frequency content from teleseismic earthquakes data were used. Hence, a viable alternative approach to imaging deep structure discontinuity is clearly necessary.

The receiver function (RF) method (Langston 1977; Ammon 1991) is known to improve depth resolution of major discontinuities such as the Mohorovičić (Moho) discontinuity or the lithosphere to asthenosphere boundary by using converted phases; and there are no inherent limitations from the existence of low-velocity layers in a complex region. RF analysis requires near-vertical incidence plane waves to elucidate the structure directly beneath a seismic station as well as broad-band (BB) seismic signals to resolve main structure discontinuities. In this paper, the waveforms in RF are determined mainly from a collection of waves converted from incident *P* waves at the Moho discontinuity including multiple reflected waves.

The Moho discontinuity is one of the most important boundaries and is accessible via deep seismic profiling, in which reflectivity and depth variations signify significant geological differences. In East Asia, RF analyses for the investigation of crustal thickness have been implemented in Korea (Chang & Baag 2005), Japan (Yamauchi *et al.* 2003; Niu *et al.* 2005), Tibet Plateau (Zhu *et al.* 1995; Tapponnier *et al.* 2001; Chen & Yang 2004), southeastern China (Ai *et al.* 2007) and Taiwan (Tomfohrde & Nowack 2000; Kao *et al.* 2002; Kim *et al.* 2004). The results for each study region are highly dependent of the tectonic and geological background involved, types of data used for analysis, data processing as well as quality control, detailed knowledge on the characteristics of fundamental assumptions used and previous experience involving RF analysis. Using short-period waveform data in RF analysis requires careful preconditioning, data selection and analysis; yet, resolution is still limited (Tomfohrde & Nowack 2000; Zhu 2000). Until the present, there have been no explicit RF studies on the spatial depth variation of Moho discontinuity beneath Taiwan Island using a more complete set of available BB data.

In this study, both waveforms and traveltimes are used in RF to determine the corresponding crustal thickness beneath each BB station. In addition, the average composition of the crustal Vp/Vs ratio κ, hence the Poisson's ratio σ, which provides an important constraint on the composition of the crust (Zandt & Ammon 1995), is estimated. Through RF analysis, first-order large-scale features based on spatial variation of Moho topography can be identified. Mori & Helmberger (1996) and Liu & Tsai (2009) showed that large-amplitude Moho reflections (SmS) produce amplified strong motions depending on local structure. Mimicking teleseismic responses with numerical calculations of the heterogeneities of the lower crust and Moho reflections indicates that by using most near-vertical incidence plane waves, recorded *PpPmP* reflections are preceded by lower crustal reverberations that terminate abruptly without scattered (coda) wavefields (Karrenbach *et al.* 1994). Therefore, for the investigation of wave responses and for tectonic structure imaging, an investigation of Moho geometry is necessary.

For a structurally complex area such as Taiwan, using both the H–κ stacking approach of Zhu & Kanamori (2000) and the enhanced two-stage weighted stacking strategy of RF phases of Zhu *et al.* (2006) can elucidate the Moho geometry. The goals of this work are to obtain better constrained results of the H and κ variations beneath Taiwan, to discover abrupt Moho depth changes in central Taiwan, to provide additional constraints on the possible tectonic processes represented by regional features, and more importantly, help to improve identification of subsequent wave phases associated with major discontinuities in strong motion simulation and prediction (Chen 2006; Lee *et al.* 2007, 2008a,b).

2 RF ANALYSIS AND H–κ STACKING

All of the data used in our RF analysis of deep crustal and upper-mantle structures were from the 'Broadband Array in Taiwan for Seismology' (BATS), established in 1998 and operated by the Institute of Earth Sciences, Academia Sinica (Fig. 1). The BATS consists of a total of 15 permanent BB seismic stations located throughout Taiwan and neighbouring islets that covers an area of 350 km $\times$ 400 km with varieties of near-surface site conditions and geological settings (Fig. 1 and Table 1). The source parameters (origin times, locations and depths) of the teleseismic events used in this study were extracted from the *USGS Weekly Report*.

The BB record database for RF analysis was obtained by: (1) carefully selecting the event records with specific magnitude, signal-to-noise ratio and azimuthal coverage; (2) preconditioning the data, including manually deleting noisy traces through visual inspection, picking the arrival time of the first break and determining the quality of the data on the basis of waveform cross-correlation within the array; (3) filtering the data to within the resolvable bandwidth, that is, from 0.1 to 3.0 Hz, on the basis of station spacing, required depth resolution and suppressing short-period scattering energy and (4) making a further evaluation by comparing the results from H–κ stacking with the result from direct stacking. A total of 1436 records, corresponding to 220 events, were carefully selected from the BATS database for our RF analysis. The criteria for selecting teleseismic events were that M_b had to exceed 5.5 and the epicentral distance had to be between 30° and 95° (Fig. 2). To extract the main features of Moho topography, a broad azimuthal coverage of teleseismic events recorded by BATS is considered first, followed by general discussions on the possibility of a dipping Moho boundary and anisotropic effects on waveforms and traveltimes.

Fig. 3 illustrates the procedures using a two-stage weighted stacking scheme for obtaining the RFs and the H–κ estimation using the data set collected at station KMNB on the island of Kinmen, just offshore of mainland China (Fig. 1). Fig. 3(a) shows both the radial and tangential components of the RF data. The RFs were extracted from three-component teleseismic records after a stable time-domain iterative deconvolution process (Ligorria & Ammon 1999). For clustering events, the stacking of radial RF traces in a predefined range of backazimuth angles involves constructive interference within specified Fresnel zones to ensure good signal-to-noise ratios and to reduce any errors because of discrepancies between the real earth and the predefined global IASPEI model structure. The individual RF traces shown in Fig. 3(a) are the result of initial stacking to increase signal-to-noise ratio.

For the second coherent stacking process, all RFs were stacked again after being corrected to a common incident angle, thereby

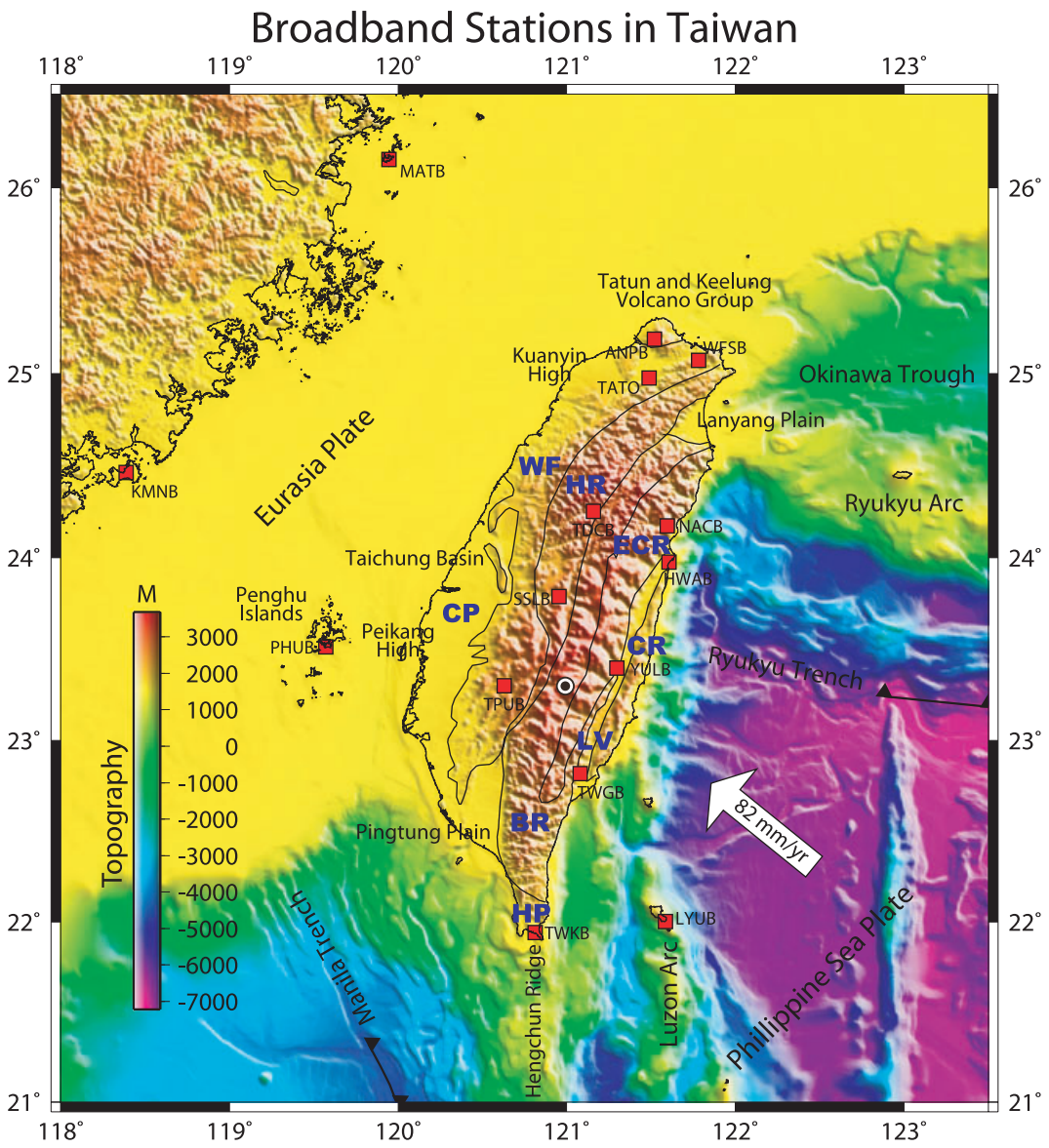

Figure 1. Topography, permanent broad-band stations and geological setting of the Taiwan region. The major tectonic provinces are labelled with black lines for Taiwan Island (Ho 1999) including**:** the Coastal Plain (CP), Western Foothills (WF), Hsueshan Range (HR), Backbone Range (BR), Eastern Central Range (ECR), Longitudinal Valley (LV), Coastal Range (CR) and Hengchun Peninsula (HP). Red boxes represent BATS three-component stations where BB data are used in this study. Station codes are shown near the red boxes with four capital letters. Ryukyu and Manila Trench mark the major convergent boundary between the Philippine Sea and Eurasian plates. The large white arrow shows the convergent direction and rate between the two plates (Yu *et al.* 1997). The peak of Yu Shan Mountain is indicated by a black dot.

placing them within the common apparent horizontal ray parameter (δp) but from different directions to reduce the effects of lateral structural variation near the station. Each averaged radial RF, as a function of the ray parameter, is gathered and shown in Fig. 3(b). The resulting averaged RFs in the p–t domain (apparent horizontal slowness versus traveltime) through declustering and coherent stacking yields enhanced Moho P-to-S_v converted phases (Ps) and subsequent multiple converted phases, including $PpPs$ and $PpSs$+$PsPs$, can be clearly identified. Noting that polarity reversal between $PpPs$ and $PpSs$+$PsPs$, which is consistent with the commonly recognized RF theoretical prediction, is clearly observable from BB data collected at station KMNB. The dominant phases, based on the assumption that plane waves are almost vertically impinging following the incidence of P waves on the radial RF, include the dominant Ps converted waves (∼3.8 s) and the subsequent multiples converted at the same Moho discontinuity. The deconvolved and enhanced radial RFs in the p–t domain were further transformed into H–κ domain using the method of Zhu & Kanamori (2000) (Fig. 3c) through stacking of sampled amplitude along the trajectories of calculated traveltimes based on the predefined ranges of κ and crust thickness. The best estimates of H and κ can be obtained through a grid search over all possible combinations of H and κ values when the amplitudes of the three phases were stacked coherently with different weighting factors (Zhu *et al.* 2006) along theoretically predicted traveltime trajectories.

In Fig. 3(b), the time separation between the P and the major converted phase Ps (t_{Ps}) from Moho discontinuity with the additional time constraints from later phases corresponds to crustal reverberations; for example, in the figure, the reflected primary multiples $PpPs$ (t_{PpPs}) and secondary multiples $PpSs$+$PsPs$

Table 1. Location of stations, *Vp*/*Vs* ratio and crustal thickness with variance. Summary of the results, including the location of the broad-band stations, the number of receiver functions used and the quality of the data for the estimated crustal parameters.

Station name	Lat./Long./Elev. (m)	*Vp*/*Vs*	*H* (km)	No. of RFs	Bed rock/geological setting	RF data quality
ANPB	25.19/121.52/825.7	1.82 ± 0.18	21.0 ± 3.0	101	Andesite/Volcanic Area	B
HWAB	23.98/121.61/0.0	–	–	17	Alluvial/LV	C
KMNB	24.46/118.39/43.0	1.78 ± 0.12	29.0 ± 1.9	118	Granite/Continental Crust	A
LYUB	22.00/121.58/40.0	–	–	41	Andesite/Volcanic Extrusion	C
MATB	26.15/119.95/75.1	1.75 ± 0.06	31.5 ± 1.5	71	Granite/Continental Crust	A
NACB	24.18/121.59/130.0	1.68 ± 0.07	38.9 ± 2.0	118	Marble/ECR	B
		1.78 ± 0.07	34.6 ± 1.8			
PHUB	23.51/119.57/50.0	–	–	22	Basalt/Volcanic Extrusion	C
SSLB	23.79/120.95/450.0	1.76 ± 0.10	52.5 ± 6.0	161	Sandstone/HR	A
		1.59 ± 0.11	40.5 ± 7.1			
TATO	24.98/121.49/53.0	1.87 ± 0.14	26.6 ± 2.5	116	Siltstone/WF	A
TDCB	24.26/121.26/1280.0	1.59 ± 0.09	36.5 ± 3.1	97	Slate/HR	B
		1.74 ± 0.15	28.9 ± 2.9			
TPUB	23.30/120.63/370.0	1.82 ± 0.14	33.6 ± 2.0	131	Siltstone/WF	A
TWGB	22.82/121.07/195.0	–	–	135	Meta-Sandstone/LV	C
TWKB	21.94/120.81/90.0	1.77 ± 0.12	33.5 ± 2.0	132	Sandy Shale/HP	B
WFSB	25.07/121.78/500.0	1.97 ± 0.18	20.6 ± 1.6	76	Siltstone/WF	A
YULB	23.40/121.30/294.7	1.58 ± 0.09	39.5 ± 3.4	100	Black Schist/ECR	A

Notes: Receiver function data quality: A, best estimated; B, best selected; C, less reliable.

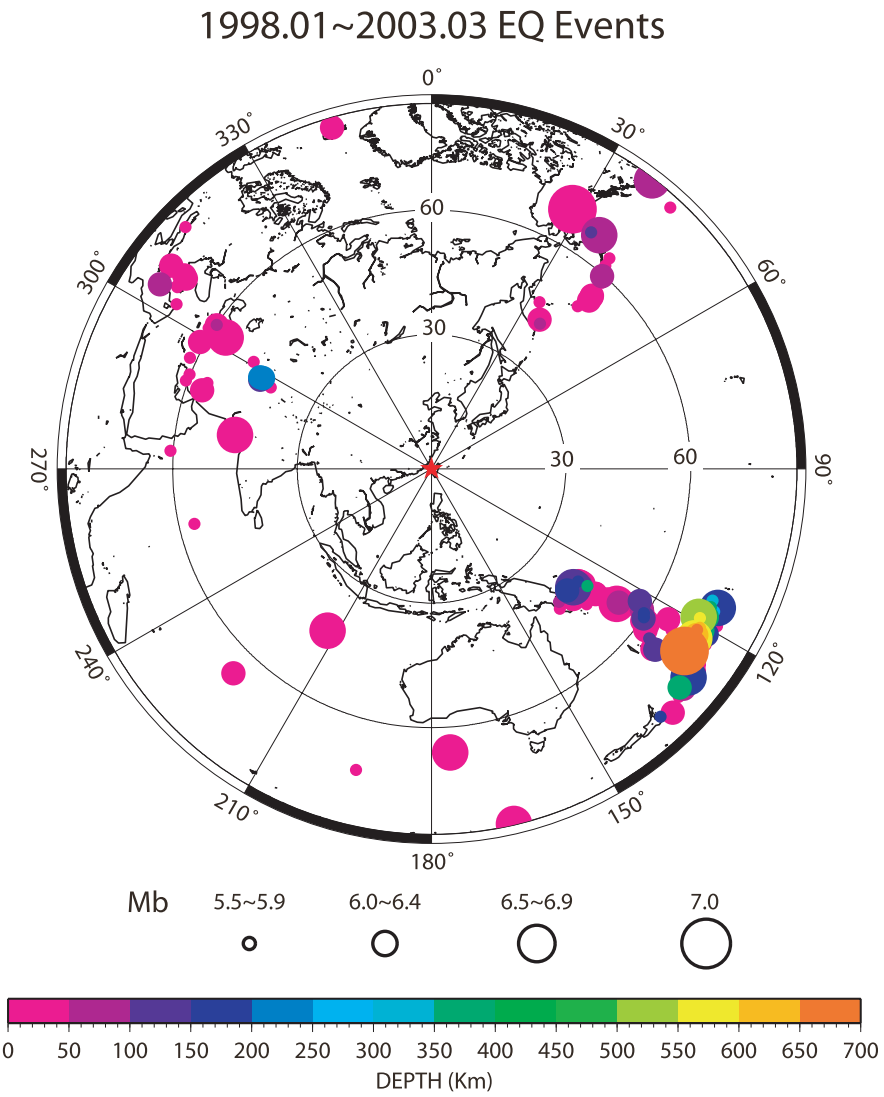

Figure 2. Equidistance projection of teleseismic event locations from 1998 January to 2003 December. The locations of the epicentres are indicated by solid circles with various values of M_b and colour-coded depth ranges. A total of 1436 records, corresponding to 220 events, were carefully used for our RF analysis.

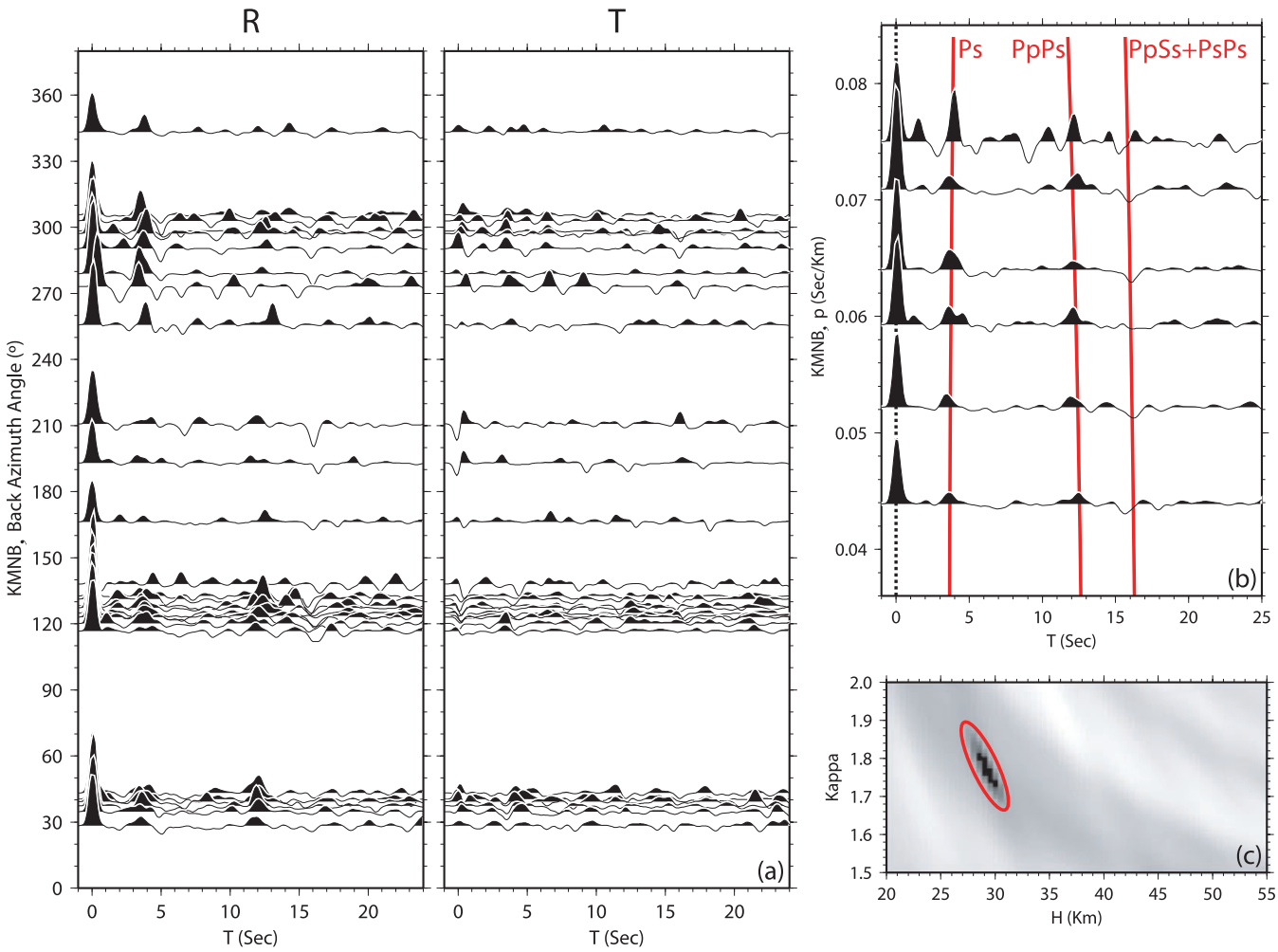

Figure 3. Illustration on the RF analysis key procedures for teleseismic data collected at station KMNB. (a) Radial and tangential RF profile arranged on the basis of the backazimuth angle. Each trace shown is the result of performing coherent stacking over averaged range of azimuth angle through declustering processes. (b) Transformation of (a) by stacking over a common incident angle and plotting in p-t profile with predicted arrival time curves (red lines) of Moho converted phases from H–κ analysis. (c) The H–κ stacking. The ellipse represents one standard deviation of uncertainty. Different weighting factors for *Ps* (0.6), *PpPs* (0.3) and *PpSs+PsPs* (0.1) are applied, respectively.

($t_{PpSs+PsPs}$) are indicated as red lines corresponding to three differential traveltime equations. For *Ps*, $H = t_{Ps}/(\sqrt{1/V_s^2 - p^2} - \sqrt{1/V_p^2 - p^2}$; for *PpPs*, $H = t_{PpPs}/(\sqrt{1/V_s^2 - p^2} + \sqrt{1/V_p^2 - p^2}$ and for *PpSs+PsPs*, $H = t_{PpSs+PsPs}/(2\sqrt{1/V_s^2 - p^2}$.

The improved two-stage weighted H–κ stacking method of Zhu *et al.* (2006) was implemented in this study by stacking coherent phases along the corresponding theoretical p–t trajectories, thereby transforming the time domain RF directly into the H–κ domain. In constructing the H–κ panel, H was first determined from the 'best' estimated t_{Ps} obtained at the maximum amplitude in the stack. In the following procedure, once the t_{Ps} differential traveltime trajectory was determined, all RFs were again stacked along the *PpPs* and *PpSs+PsPs* arrival time curves predicted from different κ values with a fixed thickness H, as determined from differential traveltime equations for t_{Ps}, t_{PpPs} and $t_{PpSs+PsPs}$. To balance contributions of amplitude from these three phases, the optimized weighting factors for *Ps*, *PpPs* and *PpSs+PsPs* are 0.6, 0.3 and 0.1, respectively. The maximum weighted sum in the second process yields the 'best' κ estimate. The approach has the advantages of not having to identify the converted phases and to pick their arrival times. Apart from this, when κ is not constrained by a *PpPs* phase, H can still be obtained from t_{Ps} by assuming a crustal *Vp*/*Vs* ratio. Accordingly, the trade-off between H on *Vp* is reduced and is less sensitive to variations in κ (Zhu 1993; Zandt *et al.* 1995; Zhu *et al.* 2006). Once the transformation to H–κ domain is done, the amplitudes no longer have a time dependency, which eliminates the ray parameters as a variable. Thus earthquakes from different distances and ray parameters can be stacked. The sum of sampled amplitudes along three p-t trajectories, the corresponding H and κ at peak**,** and the associated uncertainty ellipse reveal the best-estimated H and κ values for that station. The uncertainties of H and κ estimates were calculated based on the variance and the sharpness of the stack at the maximum. The broadness of uncertainty ellipse, illustrated in Fig. 3(c), depicts the resolving power of the corresponding crustal parameters.

At station KMNB, 118 teleseismic events were utilized and the best estimate of H is 29.0 km. The *Vp*/*Vs* ratio κ is 1.78. The corresponding σ is 0.269. The uncertainties and relative errors both in H and κ are 1.9 km (~6.5 per cent) and 0.12 (~6.7 per cent), respectively. The results for station KMNB are well constrained that can mostly be attributed to the excellent signal-to-noise ratio of

seismograms recorded at this station that was built on the granitic bedrock formation of the old and stable continental crust (Fig. 1 and Table 1).

3 CLASSIFICATION OF RF DATA AND QUALITY CONTROL

Quality control is crucial in RF analysis. Data quality and quantity are affected by the duration of deployment, frequency band used, azimuthal coverage of events, and the background noise level. Because for maximum frequency of 3 Hz, the preferred constructive interference within the specified first Fresnel zone for the *Ps* conversion point at depth of ∼30 km is within ∼10 km in horizontal distance from the station, the constructive stacking processes within a favourable epicentral distance and azimuthal coverage help to eliminate the interference effects from lateral structural variations. All RFs were visually examined after being sorted according to back-azimuth and incident angles and being compared to neighbouring RFs. To ensure high quality results, RFs with anomalous shapes or amplitudes on either the radial or the tangential component were discarded. The excellent quality of the data and well-constrained estimates of H–κ values from stations KMNB and MATB (Fig. 4a and Table 1) is largely attributed to good site conditions.

Table 1 lists the locations, geological setting of the stations and results from the H–κ analysis. While most stations are located in the mountain range, four are in the east coast (Fig. 1). The number of events used at individual stations varies from 17 to 161, depending on the length of the recording period and the background noise level. Each BATS station is equipped with a 24-bit digital data logger (Quanterra Q680, Q330 or Q-4120) and a BB sensor (STS-1, STS-2 or Trillium 240), except that TATO is equipped with a KS-36000i sensor as a joint station with the Global Seismic Network (GSN). We classified stations in three categories A, B and C based on the data quality and clearance of *Ps*, *PpPs* and *PpSs+PsPs* arrivals in the RF profiles. The combined approaches between optimized two-stage weighted stacking and strategies described in the next paragraph for quality control assure reliable H–κ estimates to constraint the construction of spatial depth variations of the 'Taiwan Reference Moho Discontinuity Model' (TRMDM) through RF analysis.

Fig. 4 represents three levels of RF data quality for stations MATB, NACB and HWAB, which are categorized on the basis of cross-correlation coefficients, visual inspection on the clearance of *Ps* waveforms concerning the existence of *PpPs* and/or *PpSs+PsPs* waveforms with polarity reversal guided by three predicted traveltime trajectories, amplitude variations for each identified phase and uncertainties associated with the H–κ estimates. The clarity of

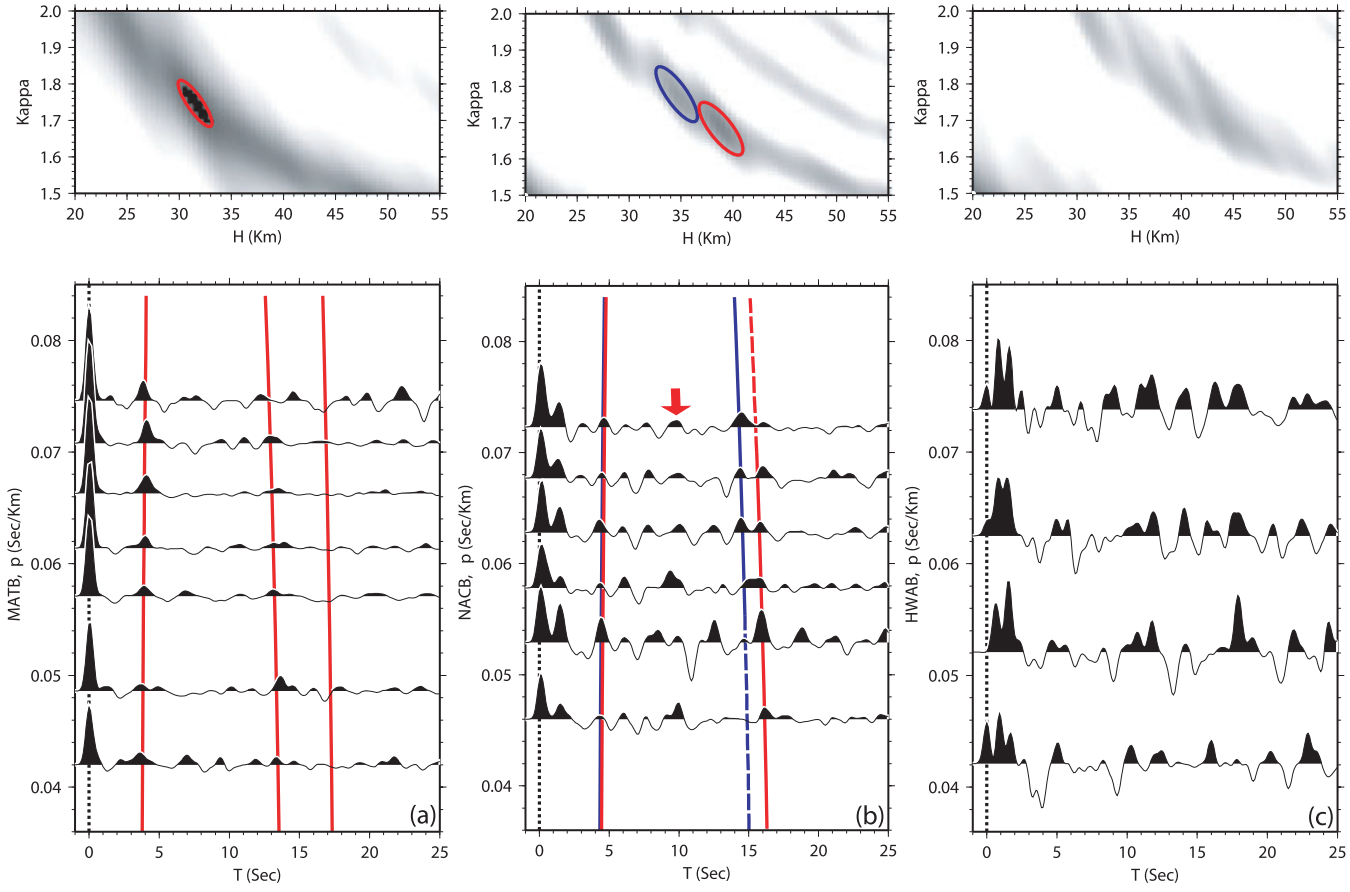

Figure 4. Classification and quality control of RF analysis. (a) Stations such as MATB are under category A and have clear Moho conversion and reverberation phases that lead to well constrained crustal parameters. (b) Stations such as NACB are under category B. Judgment based on a combination of traveltime and waveforms, regional geology features, experience with near-surface effects and adjustment of searching criteria produces possibly two reasonable results that are indicated by blue and red lines. The absence of a third coherent crustal reverberation phase or a lack of clear polarity reversal may occur for stations under category B. (c) Stations such as HAWB under category C are discarded for on the basis of data quality. At NACB station, a visible deep conversion phase (marked by a red arrow) occurs at 10 s. Also see Fig. 5 for similar RF phases from the subcrustal conversion boundary indicated at stations located in central Taiwan.

crustal reverberations, including primary *PpPs* and later multiples at each station with different categories, differ in waveform, amplitude and arrival times owing to local structures and near-surface effects.

Fig. 4(a) shows an example of a category A at station MATB which exhibits clear direct *P*, principal Moho conversion *Ps*, primary multiple *PpPs* and relatively low amplitude crustal reverberation *PpSs+PsPs* phases. The clear and coherently stacked good quality RFs at this station yield well-constrained estimates of H and κ. The *PpSs+PsPs* phase with reversed polarity at about 17.3 s is not as clear as we saw in KMNB (Fig. 3) but is still identifiable. Seven stations fall under category A (Table 1).

Fig. 4(b) shows RFs of a category B station**,** NACB**,** which has clear *P* arrival and converted Moho *Ps*, but less clear multiple phases. In addition, immediately following the direct *P*, there is a *P*-to-*S* converted phase generated at the bottom of the near-surface low velocity layer. Notable waveform change, lower amplitude and amplitude fluctuation with incidence angle on both *Ps* and *PpPs* phases (indicated by red and blue lines) appear to be mostly affected by such near-surface effects. Consequently, the H–κ stacking did not produce a clear global maximum (indicated by red and blue error ellipses). The situation can be justified from additional *a priori* knowledge for the region around each station and judgment by redefining the valid search ranges. The best estimated parameters are indicated either by red or blue lines and the marked H–κ ellipse without excluding the other maximum. Although a coherently stacked trace is helpful, the ambiguity is still mainly caused by the interference from near-surface effects and heterogeneous crust that produce notable amplitude fluctuation on *Ps* and *PpPs* reverberation phases. Therefore, for the results of category B, geological information, experience and explicit consideration of waveform information in searching for reasonable global maximums are necessary. As suggested by Crotwell & Owens (2005), we are being cautious in implementing *a priori* constraints in order to reveal the most reliable information on their bulk properties. Three other stations including ANPB, TDCB and TWKB, listed in Table 1**,** are under category B. Note that for those four stations**,** the *PpSs+PsPs* phase is either missing or does not exhibit clear negative polarity.

Fig. 4(c) illustrates the RF data of a category C station at HWAB. The recording period of this station is short and the RF data may be contaminated by the interference of signals from the shallow low-velocity sedimentary layer or sea–land interface owing to the location of the station being close to the east coast. No Moho *Ps* can be identified. The remaining two other category C BB stations, PHUB and LYUB, are also located in the nearby islets where high background noise levels and bad site conditions are suspected. A similar situation is found for station TWGB even though a total of 135 RFs were obtained, because data were largely contaminated by the near-surface effects and we were not even able to find satisfactory results through declustering and H–κ stacking. Judging from averaged RFs waveforms, three out of four BB stations under category C were significantly affected by ocean water-layer reverberations and noise, consequently such stations are all excluded.

Because of the correction to a common incident angle, the average property of crustal parameters can be obtained without detailed inspection on the azimuthal variation of waveforms and traveltimes. For category B stations, the H–κ stacking may produce multiple local maxima (Crotwell & Owens 2005) due to complex structure effects including**:** heterogeneity of the crust or azimuthal anisotropic velocity variations, the near-surface sedimentary basin, non-horizontal conversion boundaries, the presence of noise and amount of data used such that *a priori* constraints on crustal thickness or Vp/Vs ratios are needed in order to obtain the most reasonable 'true' bulk crustal parameters. To emphasis this point, Fig. 5 illustrates the complexity of RF analysis for station SSLB and more importantly, the possible common feature of notable extra subcrustal boundaries beneath adjacent stations TDCB, TAPU and YULB. The constraints on the Moho reference boundary and emphasis on the importance on their common lithospheric structure feature derived from both traveltime and amplitude information of RFs in Central Taiwan is illustrated.

Fig. 5(a) shows the result at SSLB that is located in the Hsueshan Range (HR). Its RFs are nearly free from the influence of near-surface sedimentary layer and give an anomalously large crustal thickness (52.5 ± 6.0 km) with a normal κ (1.76 ± 0.10) obtained through global searching of maximum amplitude in the H–κ panel. Besides the predicted Moho *Ps* and its multiple arrivals marked by the red lines in the p-t profile, there is a low-amplitude but evidently fairly coherent additional *Ps* phase and its crustal multiples as indicated by the blue lines and the blue ellipse in the H–κ panel. This suggests another crustal conversion interface of low impedance at a depth of 40.5 km. Similarly, the rather distinct and fairly coherent arrival approximately at ∼11.0 s in the p-t profile (indicated by a red arrow) may correspond to an extra discontinuity in the mantle lithosphere. For TDCB station shown in Fig. 5(b), the preferable possible solutions are either 36.5 ± 3.1 or 28.9 ± 2.9 km even though amplitude of RFs is less affected by near-surface effects, compared with results for NACB station show in Fig. 4(b), we cannot, however, rule out observed amplitude variation being affected by heterogeneous crust. For stations at TPUB and YULB, the crustal parameters are uniquely determined by H–κ analysis although station YULB appears to have more significant near-surface effects.

Overall, peculiar features occurred from estimated crustal parameters among the five stations in central Taiwan. From H–κ analysis listed in Table 1, stations at SSLB (Fig. 5a), YULB (Fig. 5d) and NACB (Fig. 4b) have about the same inferred crustal thickness**,** around 40 km**,** except for a slightly thinner crust at TDCB (Fig. 5b). Three out of four of the above mentioned stations have notable low Vp/Vs ratios ($\approx 1.585 \pm 0.096$) at SSLB, YULB and TDCB but with a more normal Vp/Vs ratio ($\approx 1.68 \pm 0.07$) at NACB. We did not rule out the alternative solution that depicts a slightly thinner crust of 29 ± 2.9 km with a normal Vp/Vs ratio ($\approx 1.74 \pm 0.15$) existing beneath TDCB when compared with other stations in central Taiwan. Similarly, the alternative solution at NACB station shows a thin crust while SSLB station shows the thickest crust with a normal Vp/Vs ratio. The unusual Moho depth obtained at station SSLB will be discussed separately later. Station TPUB (Fig. 5c) is located south of central Taiwan. It has a normal crustal thickness of 33.6 km. The distinct and unique high κ value of 1.82 ± 0.14 (Table 1) at TPUB station typically corresponds to the well-known Guanzihling-Dapu geothermal area.

In Fig. 5, a similar conversion phase with significant waveform amplitude at 9–11 s (red arrows) can be found from all four stations, which strongly suggests that there is a common and peculiar lithospheric feature beneath central Taiwan. Comparison of the same arrivals conversion phase with delay time of ∼9.2 s at station TDCB, ∼11 s at station SSLB**,** ∼10 s at station YULB and ∼9.2 s at station TUPB indicates that the depth variation of the identified lithospheric boundary with notable high impedance contrast correlates well with the inferred Moho topography variation prescribe from the five stations, including station NACB shown in Fig. 4(b).

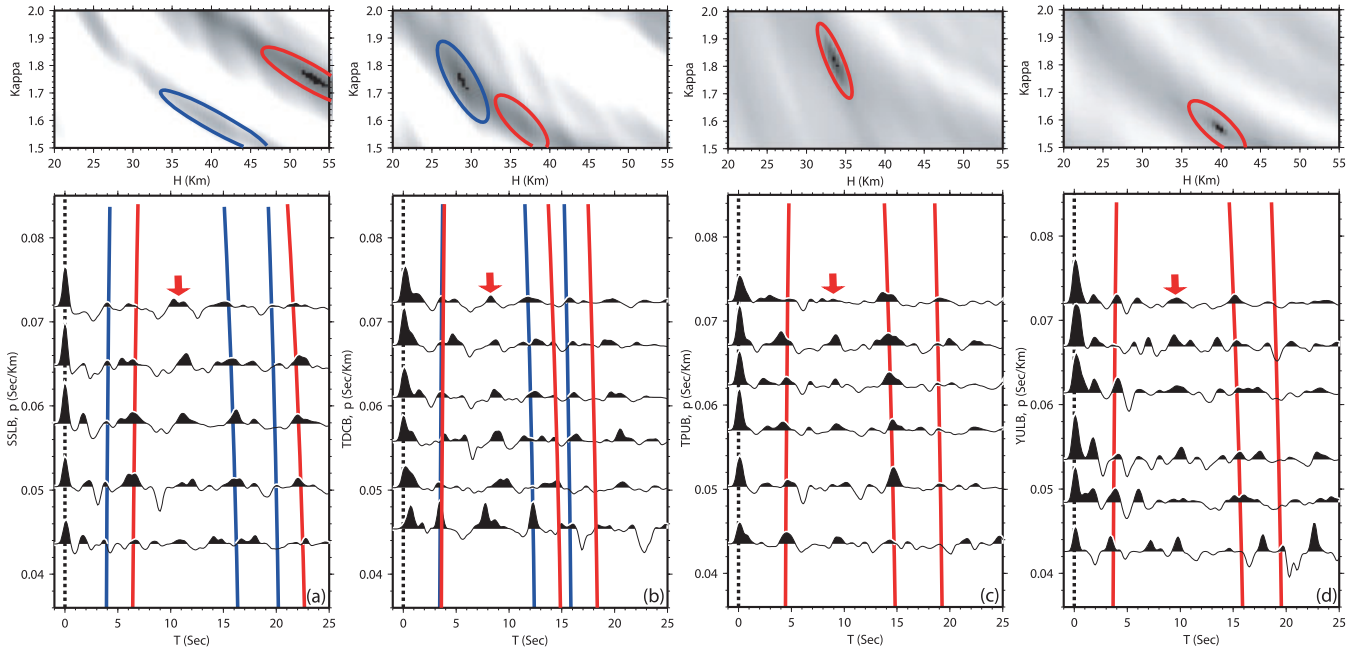

Figure 5. Constrains on Moho and subcrustal boundaries in Central Taiwan. RFs for stations**:** SSLB (a), TDCB (b), TPUB (c) and YULB (d) as a function of the ray parameters and their corresponding crustal parameters estimated from H–κ stack. The red lines represent the arrival times of the Moho *Ps*, its multiple *PpPs* and possibly *PpSs+PsPs* predicted from the best determined H–κ stack. The blue lines are the second possible solution for stations SSLB and TDCB judging from quality and quantity of the data affected by the near-surface effects and spatial correlation in terms of geological features as well as their tectonic significance. All four stations have clear wave phase at ∼10 s due to *P*-to-*S* wave conversion at a subcrustal-to-upper-mantle boundary as indicated by red arrows. Fig. 4(b) also shows a similar phase observed ∼10 s at station NACB.

4 DETERMINATION OF AVERAGE MOHO GEOMETRY

Table 1 summarizes the estimated crustal parameters along with the estimated uncertainties for all 15 BATS stations. Seven stations are under category A, which yields the best-estimated crustal parameters in the RF analysis. Four stations need constraints when seeking acceptable H and κ; therefore, these are category B stations. Most of the complications arise from geological differences associated with known magmatic activities in the backarc basin or possible existing magma chambers within geothermal areas (ANPB), the terminus of subducting slabs in the northeast (NACB) and southern (TWKB) Taiwan areas, and the possible transition zone in central Taiwan. The crustal parameters of both category A and B were adopted to construct two possible configurations of TRMDMs as illustrated in Figs 6 and 7. The corresponding 3-D perspective views of TRMDMs, which emphasize their spatially varying Moho topographic surface changes and seismicity in central Taiwan are displayed in Fig. 8 and associated Supplementary video files.

Because of sparse station distribution, the Moho-depth contours illustrated in Figs 6(a) and 7(a) only delineate the large-scale variation of Moho geometries beneath Taiwan. The variation of Moho topography changes is obtained with data from all BATS stations through a piecewise bicubic spline interpolation and minimum curvature contouring algorithm. Due to large elevation changes at each BB stations, additional receiver static correction is required to convert the crustal thickness H to Moho depth with a common datum surface corresponding to the mean sea level. The inferred Moho depth and associated uncertainty at each station are projected along the latitude- (Figs 6b and 7b) and longitude- (Figs 6c and 7c) depth profiles. Each depth section is inferred via two central projection lines drawn approximately along the NEN–SWS and WNW–ESE directions across station SSLB to emphasis Moho topography variation in central Taiwan.

In Fig. 6(a), the depth contours of TRMDM show a gradual deepening towards the southeast where the deepest Moho surface occurs in central to eastern Taiwan. The less constrained Moho depth for eastern Taiwan, typically beneath the Longitudinal Valley (LV) is due to poor station coverage. Because BATS stations are mainly distributed along NEN–SWS direction, the inferred shape of the Moho boundary along the latitude–depth profile (Fig. 6c) is better constrained and bounded by spatial station coverage. The Moho boundary (light grey dashed line) with uncertainties (short vertical error bar) through nine stations reveals a southward crustal thickening along the NS direction. Fig. 6(b) shows a longitudinal–depth profile along the central line across the midpoint between KMNB and MATB and through station SSLB. The inferred Moho configuration depicts the westward thinning and strong lateral variations of crustal thickness beneath central Taiwan.

The anomalously large crustal thickness beneath station SSLB compared with the remaining stations raises a concern about the reliability of H–κ analysis results for the station. To investigate such concern, we check earthquake seismicity from updated CWB earthquake catalogue and related studies in central Taiwan. Earthquakes are obviously a response of the accumulation of regional tectonic stresses such that locations and mechanisms allow us to explore the geodynamics of orogeny. Fig. 8(a) shows two perspective views of inferred topography variation for TRMDM (see also the supplementary Video S1) beneath stations**:** TDCB, NACB, SSLB, YULB and TPUB to emphasis the strong depth variation of TRMDM in central Taiwan. Through visualization of 3-D relocated seismicity from 1991 to 2005 of Wu *et al.* (2008), many shallow to intermediate (focal depths <20 km) earthquakes have occurred and spatial distribution of earthquakes is confined within the Moho discontinuity with no clear existence of both mantle earthquakes

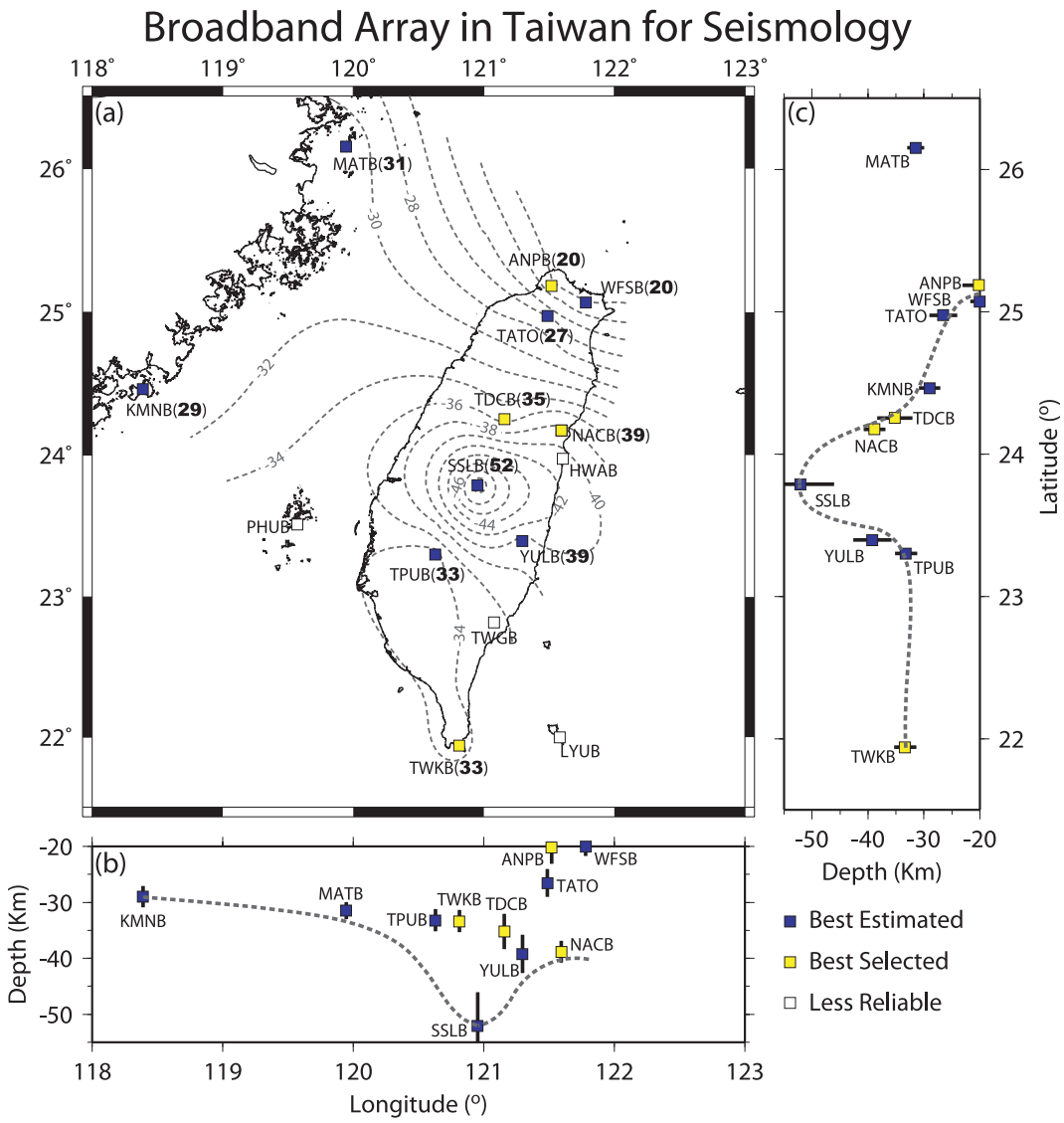

Figure 6. Map view of most preferable averaged Moho geometry and depth variations beneath Taiwan. (a) The number beside the station name is the corresponding Moho depth after elevation correction to the sea surface. The dashed line contours, denoted in light grey, outline the Moho geometry from the 11 BB stations. The blue squares are the stations with most reliable estimates of the crust parameters. Satisfactory results from four stations obtained with constraints are marked in yellow. The projected depth profiles along the longitude direction (b) and the latitude direction (c) represent the inferred Moho topographic changes. The short vertical error bars and light grey dashed line outline the topography of Moho depth changes for two central projection lines across station SSLB. For depicted Moho features and detailed discussions, see main text.

and Wadati-Benioff zone in central Taiwan. A very distinct patch of fairly shallow earthquakes cluster (see marked arrow) right underneath station SSLB. Another cluster of earthquakes, mainly associated with the 2003 December 10 Cheng-Kung earthquake and its aftershock sequences can be found to the south of station YULB. For earthquakes occurring beneath stations TPUB and TDCB, no distinctive seismicity pattern could be found except for a cluster of shallow earthquakes. The second perspective view (in Fig. 8a) clearly shows that the seismicity patch beneath station NACB appears to be associated with offshore earthquakes that occurred by the simultaneous collision and subduction of the PSP and EUP.

Due to the non-uniqueness of H–κ results at stations SSLB, TDCB and NACB, we also present an alternative Moho geometry in Fig. 7 and its corresponding 3-D perspective view in Fig. 8(b) (see also Supplementary Video S2). The Moho depth variation along the longitudinal–depth profile (Fig. 7b) beneath SSLB, YULB and TPUB is still quiet striking even though the crustal thickness at station SSLB is reduced from 52 to 40 km and the corresponding alternative Moho depths beneath TDCB and NACB also become shallow. Regardless of which the true TRMDMs should be, the compelling feature of crustal thickening and Moho geometry in central Taiwan as shown in Figs 6 to 8 should still exist.

In central Taiwan, the seismicity and Moho depth change shown in Figs 7 and 8(b) and the even more pronounced change in Moho geometry shown in Figs 6 and 8(a) may reveal important implications in terms of oblique collision features and associated mechanisms between PSP and EUP. Important to note is that the absence of deep (mantle) earthquakes approximately between the latitudes 23°N and 24°N in central Taiwan appears to occur where there exists a different ductility of rocks in the Central Range. Earthquakes along Wadati-Benioff zones in the active seismic area such as in a subduction zone apparently define a lithospheric plate that descends

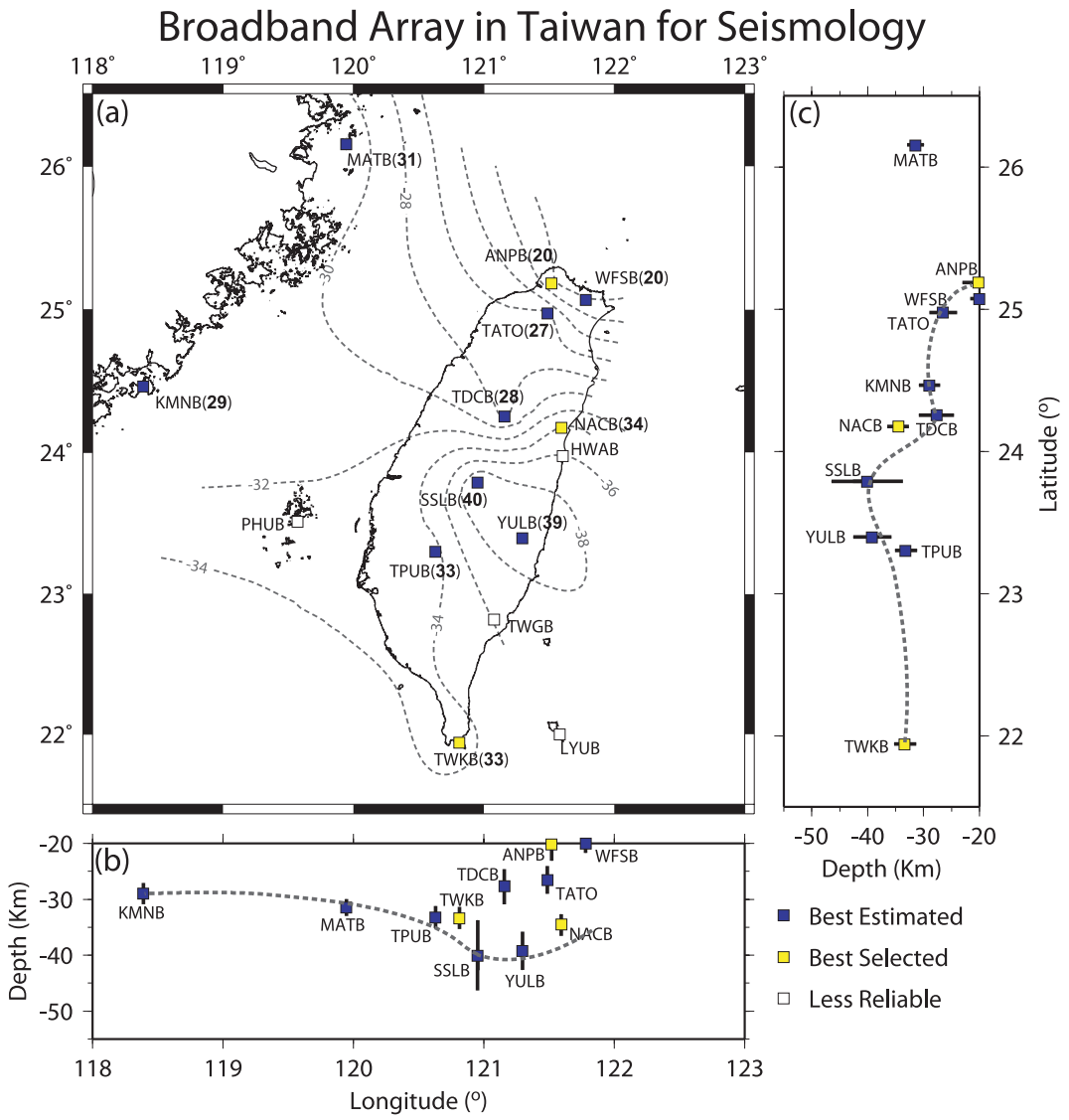

Figure 7. The proposed second possible solution on the topographic variation of 'Taiwan reference Moho discontinuity model' (TRMDM) defined by alternative solutions at stations: TDCB, NACB, SSLB, YULB and TPUB. Notable rapid Moho depth change along the latitude-profile but smooth changes along the longitude-profile may correlate with oblique collision and subduction occurring between EUP and PSP. See also Fig. 6 and Table 1.

into the mantle beneath another, overlying plate. Despite the evidence from seismicity, more detailed surveys, such as an array seismic study with dense station distribution or wide-angle reflection and refraction experiments are needed to further confirm and/or update our findings.

It is also worth noting that the RF study in southeastern China (Ai *et al.* 2007; Table 2) shows consistent crustal parameter estimation results with ours. Because only four BB stations (KMNB, MATB, NACB and TWKB) were included by Ai *et al.* (2007), no clear Moho model beneath Taiwan can be resolved from their study. Therefore this paper provides a strong link by including TRMDM with results from Ai *et al.* (2007) to construct a more complete crustal structure in southeastern China. In particular, the fairly low Vp/Vs ratio of 1.585 at stations YULB and SSLB indicates very different contrast with stations TDCB and NACB where they have an average Vp/Vs ratio of 1.76. The rather low Vp/Vs ratio may imply a small-scale crustal block or alternatively a geologically or tectonically rather significant feature may exist in that region. As indicated by Biq (1971) and Ernst (1983), the Mesozoic Plate convergence may have taken place in the LV by a westward underthrust of the oceanic eastern Yuli metamorphic belt beneath the western continental Tailuko belt on the ancient Asiatic continental margin during the subdution event. Personal communication with field structure geologist, Dr. Chung-Pai Chang, also confirms the existence of a massive granite body found near station YULB and the known existing eastern Yuli metamorphic belt within the suture zone may have caused such a result. However, we do not rule out more important implications in terms of their potential impact on possible major tectonic plate configuration change occurring or the northern extension of the subducting PSP causing such subcrust-to-upper-mantle thickening in central Taiwan.

5 DISCUSSION AND CONCLUSIONS

The method using optimized weighted stacking of RFs and H–κ analysis is applied to determine the crustal thickness (H), the averaged Vp/Vs ratio (κ) and their corresponding uncertainties. The κ value beneath each station can be converted to a Poisson ratio (σ)

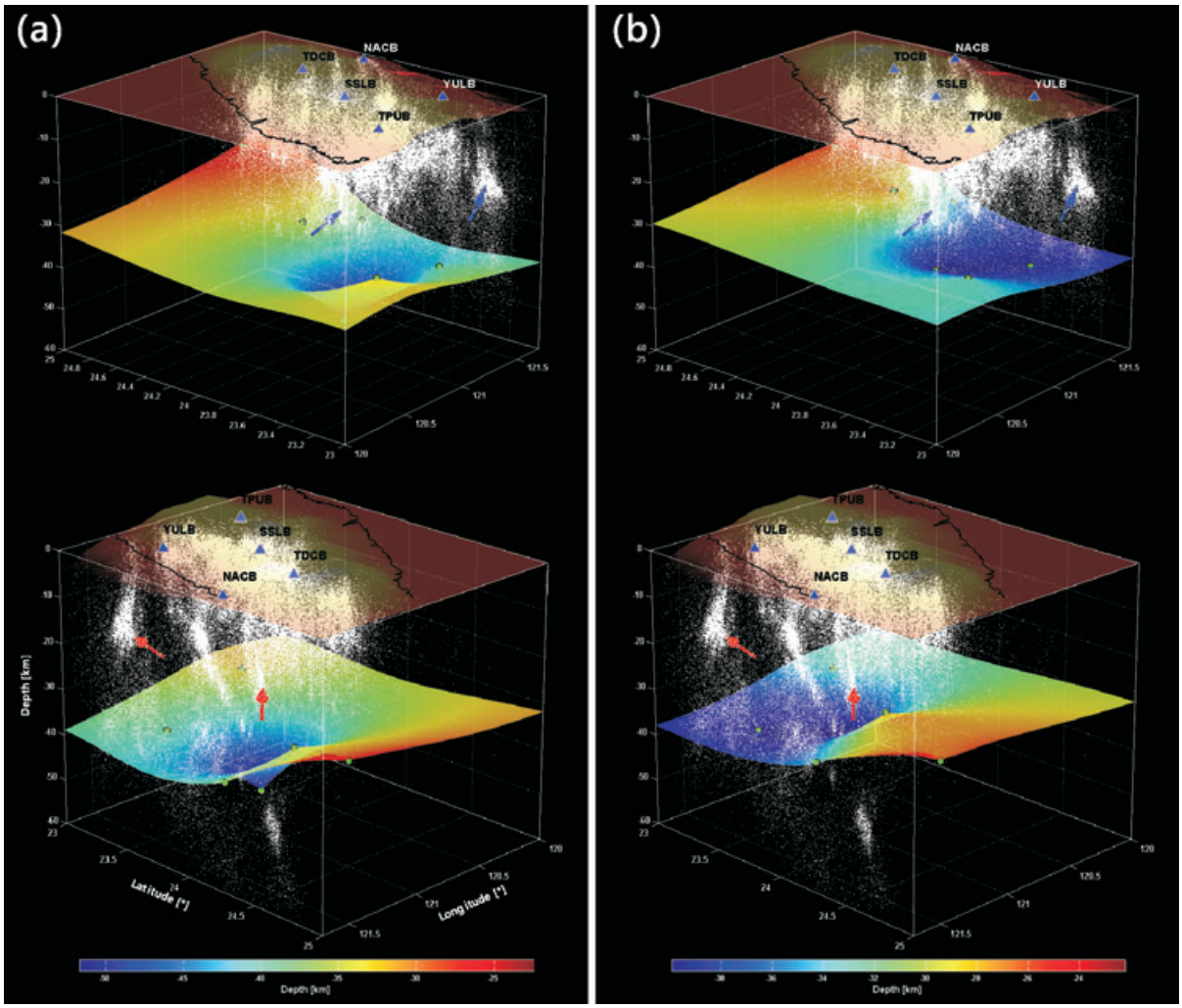

Figure 8. The 3-D perspective view of earthquake seismicity and the proposed TRMDMs constraints by stations in central Taiwan. Both (a) and (b) show the variation of Moho topography changes derived from piecewise bicubic spline interpolation among all BATS stations in Taiwan. Large depth variation indicated in (a) is mainly caused by the deepest Moho depth at station SSLB. The proposed alternative solution shows more pronounced Moho topography change across stations between TDCB and SSLB in (b). The geometry of the Moho surface is subject to change; however, the large-scale feature ought to be the same if more stations and reliable results are included.

for averaged mechanical rock properties. The crustal parameters are sometimes further constrained by known tectonic regimes while optimally searching over H–κ space whenever ambiguity occurred. The proposed spatial topographic variations of the TRMDMs are obtained from the corresponding H values after the application of an elevation correction for Earth surface topography (Figs 6 and 7).

To validate our finding, the large-scale (i.e. long wavelength and smoothed) spatial variation of the Moho boundary obtained from RF analysis is compared with tomographic studies. Overall, the Moho transition boundary, roughly outlined by the contours of Vp values ranging from 7.6 to 7.8 km s^{-1} of Rau & Wu (1995) and Kim *et al.* (2005), shows to be a generally consistent feature. For instance, Moho topography variation shows to gradually deepen towards the central to eastern Central Range and appears to exhibit deepest Moho depth in central Taiwan. Because RF analysis directly uses differential traveltimes, wave phases and amplitude information, the resolution of estimated H at each station could be higher than the indirect estimation of Moho geometry from refraction tomography studies.

Even though the general features in terms of Moho geometry are similar, the depth range of the Moho discontinuity from RF analysis is generally shallower than that previously reported from tomographic studies. Such differences may occur because the two independent approaches utilized in this study, in which the velocity model, basic physical and principle assumptions, data processing and methodology, are different. In addition, when comparing both geometry and depth variation features of TRMDMs through RFs analysis with Moho obtained from tomography inversion by Wu *et al.* (2007), the differences are even larger than the results from both Rau & Wu (1995) and Kim *et al.* (2005). The results of a pre-TAIGER experiment in 2006, in which 500-kg dynamite test shot data were collected at DiLi village close to the township of Puli in central Taiwan, also indicated that the differences are mainly from overall higher Vp and Vs velocity distribution as per Wu *et al.* (2007) such that the Moho depth is even deeper than other tomography studies have suggested (Yu 2008).

5.1 Past Moho depth determination studies

Based on the information covering waveform amplitude, differential traveltime and enhanced stacking criteria, the Moho depth derived from H–κ analysis at each BB station is generally consistent with

Table 2. Comparison of published crustal parameter models with proposed TRMDM from this study. Our study obtained more complete and reasonable results compared to other studies. The distinct differences among model parameters are highlighted in bold face and underlined numbers.

Station name	Kao *et al.* (2002) NA inversion Data criteria: not available			Kim *et al.* (2004) maximum likelihood inversion Data criteria: not available 25° < EPD < 100°, $M > 6.5$			Crotwell & Owens (2005) automated receiver function Processing Data criteria: Period: 1996– 30° < EPD < 100°, $M_b > 5.5$			Ai *et al.* (2007) *H*–kappa stacking Data criteria: not available 30° < EPD < 90°, $M > 6.0$			This study *H*–kappa stacking Data criteria: period: 1998–2003 30° < EPD < 95°, $M_b \geq 5.5$		
	Vp/*Vs*	*H* (km)	No. of RFs	*Vp*/*Vs*	*H* (km)	No. of RFs	*Vp*/*Vs*	*H* (km)	No. of RFs	*Vp*/*Vs*	*H* (km)	No. of RFs	*Vp*/*Vs*	*H* (km)	No. of RFs
ANPB	–	–	–	–	–	12	**1.60 ± 0.09**	34.0 ± 4.1	26	–	–	–	1.82 ± 0.18	21.0 ± 3.0	101
HWAB	–	–	–	–	–	–	–	–	–	–	–	–	–	–	17
KMNB	1.70 ± 0.05	31.1 ± 2.6	–	1.73	28–30	3	1.77 ± 0.01	30.0 ± 0.2	236	1.77 ± 0.06	29.1 ± 1.1	340	1.78 ± 0.12	29.0 ± 1.9	118
LYUB	–	–	–	–	–	–	2.04 ± 0.10	30.0 ± 10.0	15	–	–	–	–	–	41
MATB	1.78 ± 0.05	33.6 ± 3.7	–	–	–	–	1.73 ± 0.02	32.0 ± 1.0	65	1.76 ± 0.08	31.7 ± 1.9	141	1.75 ± 0.06	31.5 ± 1.5	71
NACB	1.77 ± 0.05	35.8 ± 2.1	–	1.73	**50–52**	7	1.68 ± 0.01	40.0 ± 0.2	172	1.79 ± 0.07	34.2 ± 2.0	244	1.68 ± 0.07 1.78 ± 0.07	38.9 ± 2.0 34.6 ± 1.8	118
PHUB	–	–	–	–	–	–	–	–	–	–	–	–	–	–	22
SSLB	–	–	–	1.73	44–46	3	1.60 ± 0.10	**68.0 ± 12.0**	124	–	–	–	1.76 ± 0.10 1.59 ± 0.11	**52.5 ± 6.0** 40.5 ± 7.1	161
TATO	–	–	–	1.73	**30–32(NE)** **36(SE)**	6(NE) 4(SE)	1.84 ± 0.04	26.0 ± 0.4	97	–	–	–	1.87 ± 0.14	26.6 ± 2.5	116
TDCB	1.80 ± 0.05	26.8 ± 2.3 (Conrad) **54.5 ± 2.9** **(Moho?)**	–	1.73	**40–50/38** **(inconsistent results!)**	7	**1.91 ± 0.09**	28.0 ± 8.5	27	–	–	–	1.59 ± 0.09 1.74 ± 0.15	36.5 ± 3.1 28.9 ± 2.9	97
TPUB	–	–	–	1.73	30–32	7	1.67 ± 0.06	**42.0 ± 2.4**	92	–	–	–	1.82 ± 0.14	33.6 ± 2.0	131
TWGB	–	–	–	–	–	–	51.0 ± 6.9	1.76 ± 0.09	72	–	–	–	–	–	135
TWKB	–	–	–	1.73	30–32	15	1.62 ± 0.04	35.0 ± 0.8	17	1.68 ± 0.06	34.5 ± 1.3	87	1.77 ± 0.12	33.5 ± 2.0	132
WFSB	–	–	–	–	–	–	1.81 ± 0.04	25.0 ± 0.8	20	–	–	–	1.97 ± 0.18	20.6 ± 1.6	76
YULB	–	–	–	–	–	–	1.60 ± 0.00	42.0 ± 0.2	150	–	–	–	1.58 ± 0.09	39.5 ± 3.4	100

the solution based on RF inversion of Kim *et al.* (2004) except at stations NACB, TDCB, SSLB and TATO.

To clarify this, Table 2 compiled all the available and published study results on determined Moho depth based on various analysis methods from BATS data in the past and compares it with our results (Table 1). At station NACB, the resolved Moho discontinuity of this study is consistent with 35.8 ± 2.1 km of Kao *et al.* (2002), Crotwell & Owens (2005) and Ai *et al.* (2007) to within 1 km, but contradict the proposed 50–52 km of Kim *et al.* (2004). At station TDCB, the proposed interface depth by Kim *et al.* (2004), based on RF inversion, is within 40–50 km but seems to have a large error and is without an explicit uncertainty estimation compared to the solutions from our study. Also, note that there is an inconsistency between the 38 km indicated in fig. 2 of Kim *et al.* (2004) and the 40–50 km discussed in the paper. One of the estimated possible depths at station TDCB for *Ps* conversion interface occur at 28.9 ± 2.9 km and is consistent with the proposed solutions of 27 ± 2.3 km by Kao *et al.* (2002) even though they think it is a Conrad discontinuity. In contrast, the proposed Moho depth of 54 km by Kao *et al.* (2002) at station TDCB deviates a lot from our result of 36.5 ± 3.1 km. However, our result could be judged to be more acceptable given that it is based on data accumulated over 5 years and strict quality control, plus the other published results shown in Table 2, overall depth variations with other stations shown in Figs 6 and 7, and the estimated uncertainties of H and κ.

At station SSLB, the proposed Moho depth of Kim *et al.* (2004) based on RF inversion is within 44–46 km. This result is more than 20 km different to that of Crotwell & Owens (2005). Kim *et al.*'s (2004) results deviate fairly largely (∼6–8 km) from our RF analysis. Such differences maybe caused by the methodology and the amount of RF used under different data selection criteria on epicentral distance and earthquake magnitude. Note that the RF data set used by Kim *et al.* (2004) is limited by the amount of good quality data collected during the early deployment stage of BATS. At station TATO, more detailed discussions on the comparison of results and possible effects on the near-surface dipping layer or anisotropy will be discussed separately.

5.2 Main features of TRMDMs in central Taiwan and their tectonic significances

From Figs 4 to 8, the complex features obtained from careful and detailed RF analysis not only reveal Moho geometry and crustal thickness variation, but also show the distinctive and consistent extra subcrustal to lithosphere scale conversion boundary at around 9–11 s outlined by stations at**:** TDCB, NACB, SSLB, TPUB and YULB.

An independent study by Chen *et al.* (2004) also shows abnormal waveform amplitudes and traveltimes anomalies beneath two stations, TPUB and SSLB, through pseudospectral modelling. Confirming their finding, the additional evidence provided from this study shows clear constraints from three other stations (in addition to TPUB and SSLB) indicating the existence of a fairly distinct conversion phase at 9–11 s (Figs 4b and 5). Chen *et al.* (2004) emphasize an existing eastern dipping aseismic slab of the subducted lithosphere from two limited observations. Our study not only confirms the main features, including crustal thickening and geometry of Moho discontinuity, but also provides more notable constraints to explicitly identify the subcrustal-to-upper-mantle structure rather than treating structure in central Taiwan as a whole heterogeneous lithospheric feature.

Typically, the main difference in our findings from Chen *et al.* (2004) is the discovery of evident thickening of crust and a consistent subcrust-to-upper-mantle boundary exist at depth approximately around 90–100 km in central Taiwan. A lack of mantle earthquakes with no obvious Wadati-Benioff zones in central Taiwan, along with the thickening of crust as well as the possible rheological behaviour change inferred from reliable spatial variation of Vp/Vs ratio (κ) (consequently Poisson's ratio, σ), and a high thermal gradient (Lin 2000) found from surface heat flow measurement (Lee & Cheng 1986) all show to be consistent features. Though on a relatively small-scale, these features, which indicate possible simultaneous mountain-building and crustal thickening, along with the on set of crustal scale conjugated faults from the 1999 September 21, Chi-Chi earthquake (Lin & Ando 2004) and seismically active area could provide an additional interpretation of possible short-term crustal dynamic processes occurring in central Taiwan.

Combining all the study results, we propose a model whereby crustal thickening may be strongly coupled with the upper-mantle lithosphere descending into the lower mantle in central Taiwan principally due to simultaneously subducting and overriding plates. However, we do not rule-out the possibility that syncollisional magmatism and detachment of a small-scale tectonic block with some degree of differential decoupling between the thickened crust and descending upper-mantle lithosphere in concert with accumulated stress promoting the occurrence of Chi-Chi earthquake whilst the whole system descends into the mantle. High-resolution regional images of the crust, Moho boundary and lithospheric features as well as their important tectonic implications would be a worthy future study in central Taiwan.

The results of the RF analysis reveal appreciable Moho topographical changes with depth down to about 52 km beneath the region of central Taiwan. Particular attention must be paid to the anomalous change in crustal thickness beneath stations SSLB located in the HR, TPUB located in the WF and YULB in the ECR. The variation in H at these three isolated BB stations across central Taiwan indicates that the depth of the Moho increases by 7–13 km over a lateral distance of less than 50 km. Moho depth changes between stations TDCB and SSLB can even vary from 4 to 24 km if the alternative thin crust model shown in Figs 7 and 8(b) is acceptable.

Apart from such a Moho topographic feature, additional evidence of relatively low κ values beneath both stations YULB and SSLB and corresponding fairly strong Vp/Vs beneath stations TDCB and NACB (Table 1) create a rheological deformation contrast. Such results may indicate trace evidence of how complex tectonic evolution promoting processes of orogeny in central Taiwan involve differential crustal shortening and crust-to-upper-mantle scale thickening and that these processes are strongly associated with the initial collision between the PSP and EUP in southern Taiwan before extending northward.

Judging by the compelling thick crust beneath SSLB and YULB and the distinct differences in lithologic properties (Table 1), the structures beneath these two stations may exhibit different ductility of rock due to their origins. Hence, determining the likely causes of abrupt changes in crustal parameters across different tectonic boundaries in central Taiwan is crucial for future detailed wide-angle refraction and reflection seismic investigations.

5.3 Consistent results from the straight stack of RFs

Fig. 9 shows the results from direct stacking with time corrections for all available radial RFs at all 15 BB stations used in

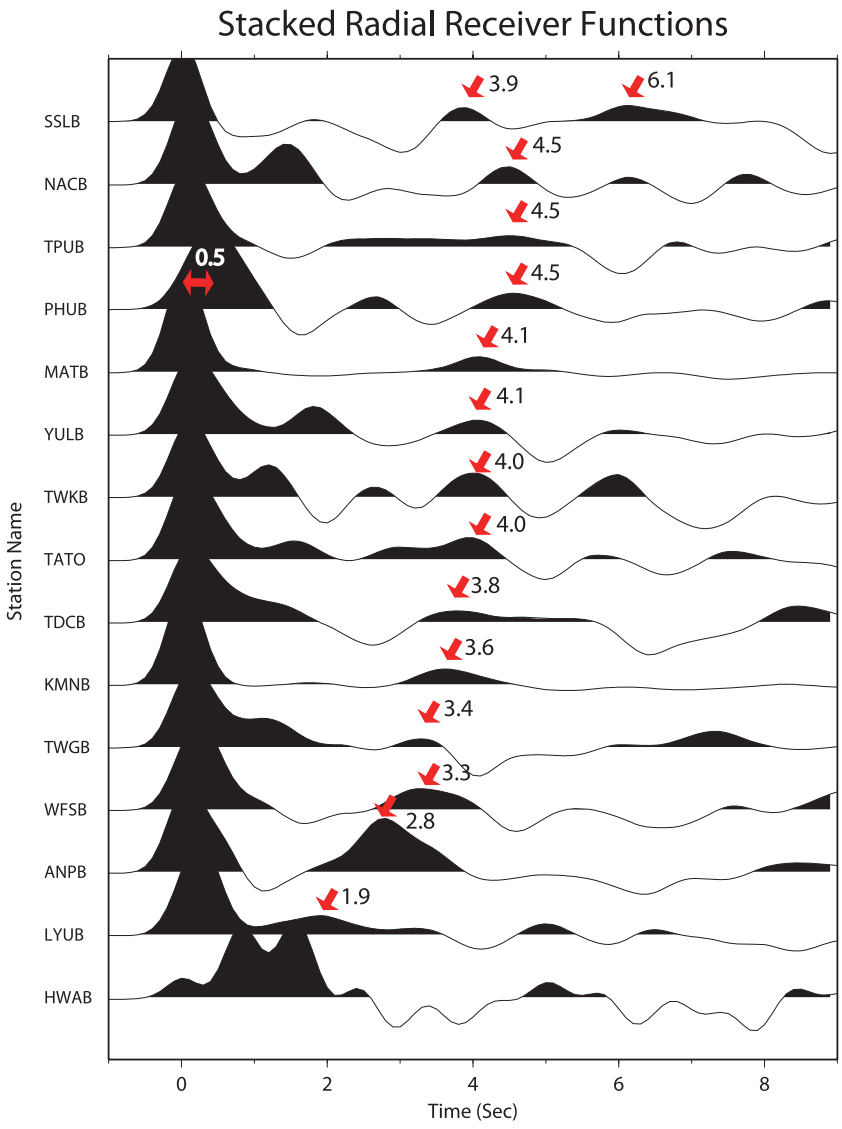

Figure 9. Stacked receiver functions at all 15 broad-band stations arranged (from top to bottom) in order of decreasing Moho *Ps* arrivals. Arrows and associated numbers indicate the identified *Ps* phase and arrival time. SSLB station shows an existing pair of possible discontinuities at depths of 40.5 ± 7.1 km (3.9 s) and 52.5 ± 6.0 km (6.1 s). Station ANPB is located inside the Yang Ming Shan–Tatun Volcanic Nature Park. The clear broadening of *Ps* phase may be associated with the existing magma chamber. At station PHUB, apparent 0.5 s shift is caused by a short deployment period, local geology conditions or strong water column reverberations. At station LYUB, the direct stack producing an unclear Moho reflection is mainly caused by both site conditions and strong water column reverberations.

this study. Confirmation on the importance of data quality control and the consistency between analysis from straight stacked traces and results from estimated H and κ values for each station are emphasized here. The corresponding Moho conversion phases from direct stacked traces also reveal a general westward crustal thinning and southward thickening with strong lateral changes in terms of Moho depth variations for central Taiwan.

The helpful direct stacking approach is also demonstrated for the station at PHUB. The stacked trace at PHUB has apparent shift of about 0.5 s due to a relatively low number of recorded events and possible interference from extrusive basaltic lava and the ocean layer; however, a possible Moho conversion phase at 4.0 s after time correction is still visible even though we decided to abandon the results from H–κ analysis for that station. For stations with good data quality, the directly stacked RF with picked arrival times between 3.3 and 4.1 s shown in Fig. 9 confirms consistent results from H–κ analysis. Even though near-surface effect may exist, the consistent results with the additional constraint from direct stacking assured that the stacking strategy is applicable so long as data selection and quality control are excellent. This means such an approach, though relatively simple, is useful even in a complex tectonic environment such as Taiwan.

Three out of four stations (except station PHUB) have relatively large arrival times (≥4.5 s) indicating more appreciable Moho geometry and a deeper conversion boundary at 9–11 s (Fig. 6) even though another possible solution (Fig. 7) is also proposed from H–κ estimation. Two possible solutions of H at station SSLB can also be confirmed from stacked traces with corresponding phases at 3.9 and 6.1 s. For stations with *Ps* phase arrival less than 3.3 s, stacked RF at station ANPB not only show a relatively early arrival time of 2.8 s, but also show fairly obvious broadening of the waveform and large *Ps* phase amplitude, which further indicates that some caution is required in searching for reasonable crustal parameters. Note also that such a common feature as waveform broadening phenomena

can be observed both in stations ANPB and TPUB where well-known geothermal and magmatic activity exists in both areas.

Data from stations HWAB and LYUB should be discarded, which is consistent with our H–κ analysis, because a relatively low number of RFs can be used due to bad site conditions, and unclear and erroneous Moho conversion phases. We strongly recommend reselection of recording sites for both stations. The less significant results from direct stacking of 135 RFs at station TWGB also confirm our decision to abandon H and κ values simply because data were largely contaminated by near-surface effects and the relatively low amplitude observed for the conversion phase at 3.4 s.

5.4 Compare results with EARS and non-isostatic equilibrium

The results from our H–κ analysis of RF from the BATS data set listed in Table 2 were also compared with the results publicly available over the Internet under the EARTHScope Automated Receiver Survey, the EARS (*cf*. http://www.seis.sc.edu/ears/; browse network list for comparison), in which an automated RF processing system based on the idea of Standing Order for Data (SOD, hhtp://www.seis.sc.edu/SOD/) is introduced by Owen *et al.* (2004) and Crotwell & Owens (2005).

From EARS, a notably large Moho topographic change occurs at station SSLB. This finding is also consistent with our study. Seven out of 15 stations have similar results and are within permitted uncertainties. From EARS, solutions at two stations TWGB and LYUB with large standard deviations are available; however, results from these stations were discarded in this study because of poor solutions due to noise contamination (Fig. 9) or even non-convergence in H–κ analysis. Large differences occurred mainly at stations SSLB, TPUB and ANPB; however, results for both stations TPUB and ANPB by Crotwell & Owens (2005) are not constrained by the known geothermal and magmatically active areas being discussed in this paper**,** consequently the inferred κ values may not be acceptable. From EARS, station SSLB has an anomalous thick crust of 68 km with a standard deviation of 12 km. Two possible crustal thicknesses beneath SSLB (Fig. 5 and Table 1) have been proposed. Although**,** for SSLB, the corresponding errors are still relatively large compared with other stations, the results appear to be more acceptable from our analysis because of careful quality control via visual inspection and selection of data, as well as processing, comparison with direct stacked traces and detail evaluation of near-surface effects.

Crustal thickness beneath central Taiwan gradually increases in an eastwardly direction to about 50 km beneath the Eastern Central Range (ECR) that is consistent with results from a dense linear seismic array deployed in the Western Foothills (WF) for earthquakes occurring in the Coastal Range (CR) by Lin (2005). The significant horizontal offset of ∼35 km between the peak of Yu Shan Mountain (Fig. 1) and the deepest crust in the SSLB region with apparent rapid depth change of the Moho discontinuity suggests that crustal deformation has not yet reached isostatic equilibrium (Yen 1998; Lin 2005). Uncertainties pertaining to estimates of Moho depths may be related to unconstrained errors from simplified crustal structures. However, the general pattern of the eastward-dipping Moho discontinuity across central Taiwan (Figs 6, 7 and 8) remains the same.

Observations of both Moho and subcrustal lithospheric boundary conversion phases shown at stations**:** NACB, TDCB, SSLB, TPUB and YULB provide fairly strong evidence of the existence and shape of the Moho discontinuity across central Taiwan and the important tectonic implications for Taiwan orogeny. Whilst the general geometry of the Moho surface may be improved with better resolution via a reduction in station spacing, the general trend for such a large-scale feature ought to remain the same.

5.5 Comparison of Moho depth determined from TAICRUST experiment in 1995

RF responses beneath Taiwan BB data from BATS are, in general, fairly complex on both the radial and transverse components due to data quality, complex tectonic setting and significant near surface and ocean layer effects. Therefore, data selection by cross-validation between data sets and adjacent stations, careful processing, accumulated experience and identification of Moho phases associated with crustal reverberations are critical in H–κ analysis. A Moho depth of 34 km at station TPUB is consistent with preliminary results from the Southern Cross-island Highway profile (L2) of the TAICRUST experiment (Yeh *et al.* 1998). The crustal thickness obtained by H–κ stacking at station TDCB has been better constrained than that of Kim *et al.* (2004, see previous discussion). However, crustal thickness at station NACB is quite inconsistent with the results from RF inversion (Kim *et al.* 2004; Table 2).

Despite questions regarding insufficient energy penetration from the offshore airgun source, low signal-to-noise ratios, scattering that affects the identification of reflection phases, the uncertainty involved in 3-D to 2-D projections, or even more seriously, the possibility of no constraints from ray coverage, the crustal thickness obtained from the TAICRUST wide-angle deep seismic profiling near station NACB (Shih *et al.* 1998) is 45 km and has a 6–10-km depth difference (Table 1). In reference to the crustal thickness derived from the TAICRUST project, RF analysis results show shallower and smaller depth differences compared with the results of Kim *et al.* (2004), which have Moho depth at 50–52 km with a deeper 11- to 17-km depth difference. The preliminary results from the use of the limited BB data set of Kim *et al.* (2004) not only give the deepest Moho depth as being at station NACB among all the stations they analysed, but also provide a completely different solution from other published studies listed in Table 2.

On the contrary, at station SSLB, we obtained two possible Moho depths one of which is consistent with the TAICRUST experiment. However, we still cannot rule out H at 53 km as being a possible depth because of the problems with the TAICRUST experiment mentioned previously. The NACB station is located near the most active and complex collision area of Taiwan while the SSLB station is located near Central Taiwan with its own distinctive seismicity pattern (see previous discussion and Fig. 8). It is also close to the Chelungpu fault where the Chi-Chi earthquake occurred on 1999 September 21. The different results might be due to miss identification of the Moho and/or possibly slab phases from collected data and/or the difference in methods. To investigate these discrepancies, we have carefully checked all the RFs by varying the stacking criteria and associate H–κ results at each station, the results of which further confirm our results. Therefore, evidences from other types of geophysical data, more advanced data analysis approache**s** and more rigorous crustal-scale reflection profiling and refraction/wide-angle reflection surveys are required to obtain more definite measurements on crustal thickness.

5.6 Effects on crust heterogeneity, dipping Moho boundary and anisotropy

The sparsely distributed BB stations in Taiwan are not suitable for resolving the complicated effects of subsurface structures. Based on the approach and results of this study, only prominent features can

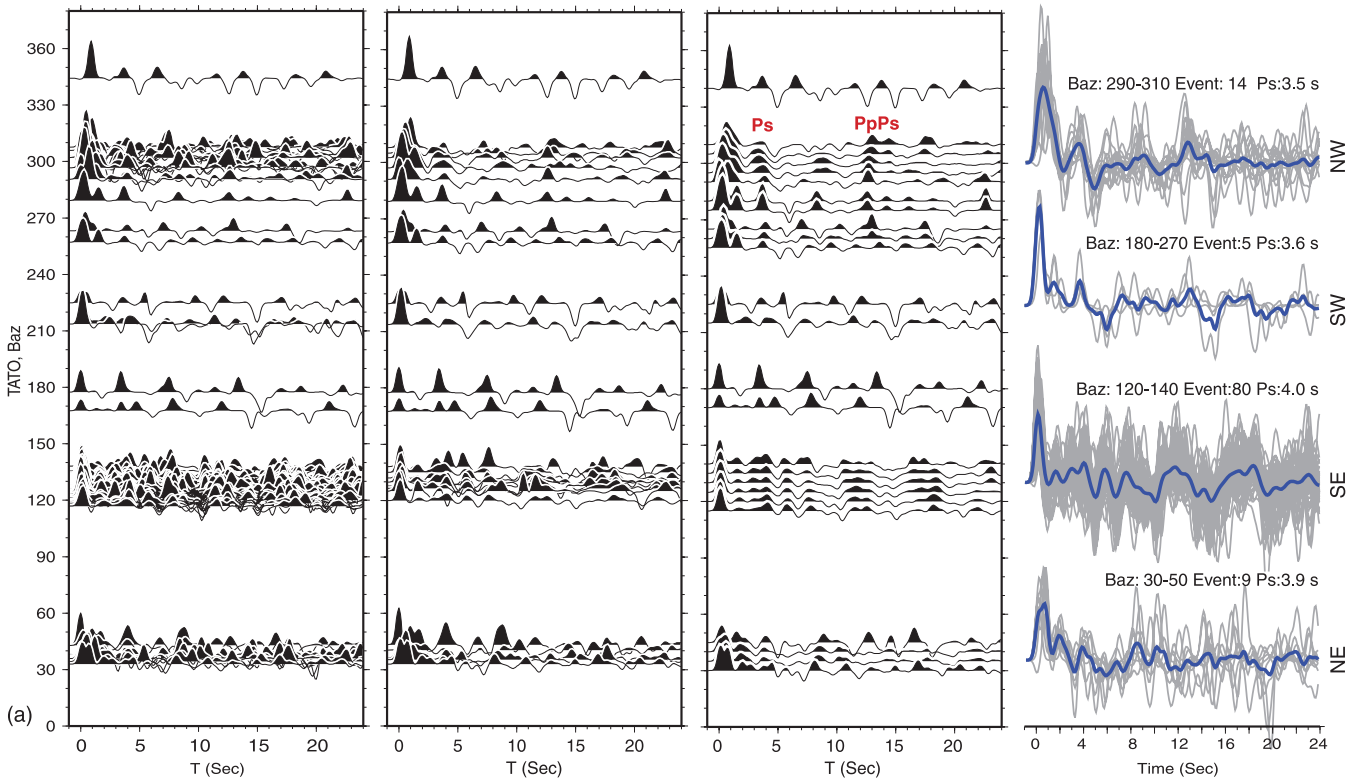

Figure 10. Radial-component receiver functions profiles for TATO station. (a) From right- to left-hand panels show the profiles through different stacking strategies: the original RFs, averaged over the combination of backazimuth (BAZ, therefore epicentral distances) and apparent incidence angle (therefore apparent slowness parameter), and stacking by an adaptive beamforming scheme with an incremental beam width of 5°. The last panel shows the representative RFs (blue traces) obtained with events from four directions within the limited ranges of BAZ angle. The wide range of events from the SW may have unreliable stacked RF trace. Similar but slightly different RFs are apparent from events of similar and different azimuths. (b) The best determined crustal parameters obtained from H–κ analysis show the same results, where H is 26.6 km and κ is 1.86. The error ellipses indicate larger uncertainty in κ while the uncertainty for H is smaller. Regardless of the stacked RFs chosen, stable and robust results can be obtained from H–κ analysis.

be explored. However, according to published seismicity patterns in NE and blur imaging in S Taiwan and other tomographic studies, the existence of a significant subducting slab is well known. Therefore, concerns pertaining to the possibility of azimuthally varying RF responses reflecting complex subsurface structures, an isotropic dipping Moho boundary or anisotropic effects on waveforms and traveltimes, and their trade-offs are discussed and compared using stations in northern Taiwan.

Station TATO, a joint station with the Global Seismic Network (GSN), is located on the edge of the Taipei sedimentary basin. The fairly intensive study on RFs at TATO by Kim *et al.* (2004) strongly suggests that both dipping and anisotropy effects could be dominant. To verify and to emphasize the validity of H–κ analysis used in this paper, the robustness of the stacking approach is demonstrated from several aspects. First, by examining the direct-stacked RF at TATO shown in Fig. 9, the waveform for the direct P (at $t = 0$ s) is apparently interfered by reverberation followed by Ps arrival, which has normal amplitude compared with adjacent stations including ANPB and WFSB. The amplitude of the Ps waveform is apparently contaminated by a precursory reverberating signal caused by basin amplification and resonance effects but it still can be identified fairly easily. Second, Fig. 10(a) compares the results at station TATO from different stacking strategies including: the original spatially distributed teleseismic events (left most panel); stacked data by simultaneous consideration of impinging waves from both common backazimuth angle and apparent horizontal slowness (second panel); stacked data by an adaptive beamforming scheme with constant beam width (third panel); and four representative stacked traces from the four major ranges of backazimuth angles (right most panel). The adaptive beam width used is 5° in order to reduce the sensitivity of anomalous signals from certain directions of arrival. Due to limited graphic space, stacked data with a common incidence angle (common δp) gives a similar result and is therefore not shown. For all the data, true amplitude is displayed to emphasis the relative amplitude differences among**:** direct P, reverberations, converted Ps waves and later arrivals. Finally, Fig. 10(b) shows that the solutions from H–κ analyses indicate consistent results in the estimation of crustal parameters.

In Fig. 10(a), RF profiles show alterations of stacking criteria through different backazimuth, incidence angles and beam widths to clearly show the progressive enhancement of Ps arrivals. The representative stacked trace from the four major backazimuth angles (right most panels) has features including: (1) Notable interferences from basin effects that can be observed within 5 s. The Ps phases between each stacked trace have arrival time differences of up to 0.5 s. (2) Most incoming teleseismic events are within a limited backazimuth angle range of 20° except for stacked traces from widely distributed events from the SW direction. (3) A different number of events is used to form one stacked trace. Both stacked traces for events from the NW and SE directions have reasonable stacking numbers and produce more representative waveforms. Relatively small event numbers and wide backazimuth angle ranges, such as events from the SW direction may produce unreliable waveforms caused by stacking artefacts. (4) The stacked trace from the NW

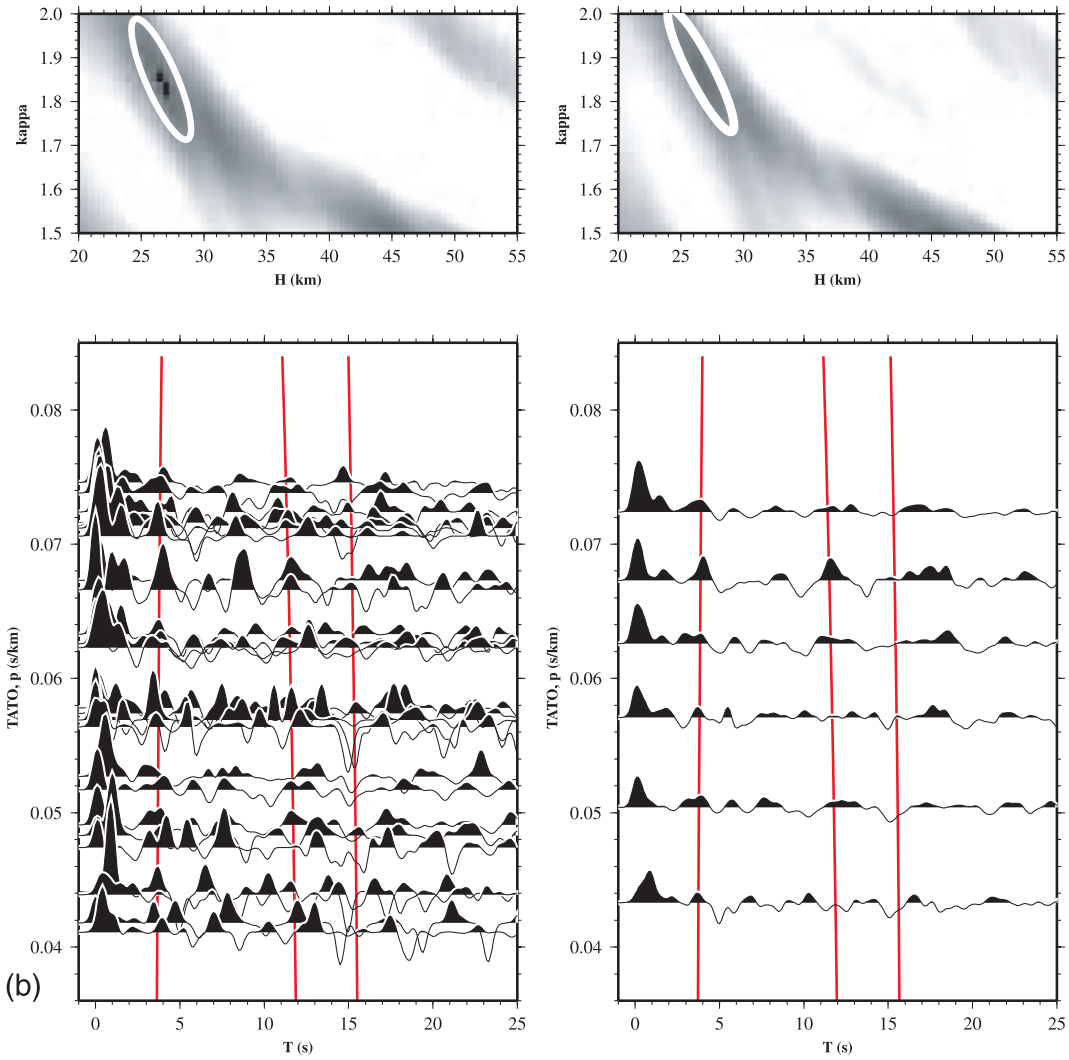

Figure 10. (*Continued.*)

direction show appreciable pulse broadening and lack of clear *Ps* waveforms. (5) The stacked trace represents events from the SE direction showing relatively sharp *P* arrivals but without clear *Ps* waveforms. Relative low amplitude and even ambiguous *Ps* phases may indicate a low contrast Moho boundary or due to effects caused by the dipping layer(s). When comparing the direct stacked trace at the TATO station (Fig. 9) with the four separate traces from four different backazimuth angles, the waveform and amplitude of the *Ps* phase is significantly affected by reverberations generated by near-surface effects. Judging by the large amount of events from the SE and NW directions with low amplitude *Ps* conversion phases, the high amplitude Moho phase at the TATO station shown in Fig. 9 is most likely caused by a combination of amplification effect and complex laterally varying crustal heterogeneity.

Although crustal heterogeneity can be identified, results from different stacking criteria all show consistent phenomena in enhancing both the visibility of *Ps* Moho conversion phases and near-surface basin effects. In Fig. 10(a), comparison of the RF profiles from the original (left most panel) to adaptive beam stacked profiles (third panel), a large number of earthquake events from the SE are apparently affected by basin reverberations but their *Ps* phases are progressively enhanced and still become visible. In addition, for earthquakes with BAZ ranges from 260 to 310, although some arrival time differences may exist in *Ps* phases, long propagation distances enhance the apparent moveout curvature of *PpPs* arrivals indicating some effects relating to a dipping layer. Therefore, such enhanced data sets (third panel) using an adaptive beamforming scheme is helpful in determining crustal parameters and the discrimination of dipping boundaries within a particular range of incoming events. Besides the enhancement of *Ps* phases, Fig. 10(b) illustrates almost exactly the same results from H–κ analysis for data sets via different stacking criteria. Therefore, the stable and robustness of stacking approaches and H–κ analysis for obtaining reasonable crustal parameters can be clearly demonstrated even in areas with apparently existing dipping boundaries. Regardless of the azimuthal variation of waveforms and traveltimes, while interference from near-surface and basin resonance and amplification effects is observable, stacking over a large number of events is effective in terms of producing both acceptable H and κ values.

In Fig. 10(b), the apparent time difference from different incidence angles can be observed from both the original data, and stacked data set. Such a difference may be attributable to crustal anisotropy, however, to clearly differentiate such effects from lateral heterogeneity, might be difficult using the stacking approach due to inherent ambiguity, and therefore the study of anisotropy by studying transverse components is beyond the scope of this paper.

For comparing results obtained from different global 1-D reference models (IASPEI, AK135) and a local tomography model, the estimates agree well for most of the grade-A and B stations with acceptable differences within the uncertainty levels. Similar conclusions were obtained for other BB stations including ANPB and WFSB in northern Taiwan.

Because available BB waveform data mostly recorded earthquakes from the SE direction, full azimuth coverage is limited for permanent BB stations in Taiwan. Therefore, only radial RFs of layered crustal structures beneath each station are analysed. Further detailed analysis must be performed to refine the Moho geometry and crustal composition through better BB station coverage by reducing interstation spacing, improving site selection and increasing the amount of data accumulated. Although geographically stations TATO, ANPB and WFSB are close to each other, their RFs can be different. This may indicate significant lateral variation of crustal structure in northern Taiwan. Separate studies on the effects of dipping boundaries, anisotropy and more detailed intercrustal boundaries using more elaborated RF analysis methods should be considered for future research. The first-order feature indicating relatively shallow Moho depth could still be related to the western terminus of the Okinawa Trough, backarc opening behind the Ryukyu Trench and known volcanic activity in the Yang-Ming and Hsin-Shui geothermal areas**,** which indicate high geothermal heat flow and thin crust ($\sim$23 km).

In summary, RF analysis with optimized weighted H–κ stacking is effective. It has the advantage of being a simple method for exploring first order features such as Moho geometry and crustal thickness in Taiwan. Transmission tomography or surface wave inversion studies may provide alternative approaches to resolving lateral velocity variation of deep structures from refracted rays. By contrast, RF analysis may reveal prominent features and better vertical resolution through use of both waveform (amplitude) and traveltime information when structures are not complex and when careful study of RFs is made. The best estimated regional mean Moho depth is 33.5 $\pm$ 2.9 km. The complexity of the subduction system in central Taiwan may be strongly related to crustal detachment, realistic rheological behaviour of the lower crust and the strength of crust–mantle coupling.

ACKNOWLEDGMENTS

We are grateful to Dr Wen-Tzong Liang and the technical staff of the Data Management Center of the Institute of Earth Science (DMC-IES), Taiwan, for managing the high-quality broad-band data. The authors would also like to thank critical review by Jer-Ming Chiu and the National Science Council, Taiwan, for financially supporting this research under grant contract number NSC92–2119-M-194–008.

REFERENCES

Ai, Y., Chen, Q.F., Zeng, F., Hong, X. & Ye, W., 2007. The crust and upper mantle structure beneath southeastern China, Earth Planet, *Sci. Lett.,* **260,** 549–563.

Ammon, C.J., 1991. The isolation of receiver effects from teleseismic P waveforms, *Bull. Seismol. Soc. Am.,* **81**(6), 2504–2510.

Biq, C., 1971. Comparison of mélange tectonics in Taiwan and some other mountain belts, *Petrol. Geol. Taiwan,* **9,** 79–106.

Chang, S.J. & Baag, S.R., 2005. Crustal structure in southern Korea from joint analysis of teleseismic receiver functions and surface wave dispersion, *Bull. Seismol. Soc. Am.,* **95**(4), 1516–1534.

Chemanda, A.I., Yang, R.K., Hsieh, C.H. & Groholsky, A.L., 1997. Evolutionary model for the Taiwan collision based on physical modeling, *Tectonophysics,* **274,** 253–274.

Chen, P.F., Huang, B.S. & Liang, W.T., 2004. Evidence of a slab of subducted lithosphere beneath central Taiwan from seismic waveforms and travel times, *Earth planet. Sci. Lett.,* **229,** 61–71.

Chen, W.P. & Yang Z., 2004. Earthquakes beneath the Himalayas and Tibet: Evidence for strong lithospheric mantle, *Science,* **304,** 1949–1952.

Chen, H.W., 2006. Prestack parallel computing of dispersive and attenuating medium, *Terr. Atmos. Ocean. Sci.,* **17**(1), 203–231.

Crotwell, H.P. & Owens, T.J., 2005. Automated receiver function processing, *Seismological Research Lett.,* **76,** 702–709.

Ernst, W.G., 1983. Mountain-building and metamorphism, a case history from Taiwan, in *Mountain building,* pp. 247–256, ed. Hsu, K.J., Academic Press, London.

Ho, C.S., 1999. *An introduction to the Geology of Taiwan, Explanatory Text of the Geologic Map of Taiwan,* Central Geol. Surv. Minist. of Econ. Affairs, Taipei, Taiwan.

Hsu, S.K. & Sibuet, J.C., 1995. Is Taiwan the result of arc-continent or arc-arc collision? *Earth planet. Sci. Lett.,* **136,** 315–324.

Hwang, R.D. & Yu, G.K., 2005. Shear-wave velocity structure of upper mantle under Taiwan from the array analysis of surface waves, *Geophys. Res. Lett.,* **32,** L07310, doi:10.1029/2004GL021868.

Karrenbach, M., Ritter, J. & Fuchs, K., 1994. Wave propagation in the heterogeneous lower crust –Finite difference calculations: SEP80, 563–588.

Kao, H., Chang, C.H. & Chen, R.Y., 2002. Receiver function analysis for broadband stations in Taiwan, CWB Annual Report: MOTC-CWB-91-E-07.

Kim, K.H., Chiu, J.M., Kao, H., Liu, Q. & Yeh, Y.H., 2004. A preliminary study of crustal structure in Taiwan region using receiver function analysis, *Geophys. J. Int.*, **159,** 146–164.

Kim, K.H., Chiu, J.M., Pujol, J., Chen, K.C., Huang, B.S., Yeh, Y.H. & Shen, P., 2005. Three-dimensional V_P and V_S structural models associated with the active subduction and collision tectonics in the Taiwan region, *Geophys. J. Int.,* **162,** 204–220.

Langston, C.A., 1977. The effect of planar dipping structure on source and receiver responses for constant ray parameter, *Bull. Seismol. Soc. Am.,* **67**(4), 1029–1050.

Liu, K.S. & Tsai, Y.B., 2009. Large effects of Moho reflections (SmS) on peak ground motion in northwestern Taiwan, *Bull. Seismol. Soc. Am.,* **99**(1), 255–267, doi:10.1785/0120080258.

Lee, C.R. & Cheng, W.T., 1986. Preliminary heat flow measurements in Taiwan, presented at the Fourth Circum-Pacific Energy and Mineral Resources Conference, Singapore.

Lee, S.J., Chen, H.W. & Huang, B.S., 2008a. Simulation of strong ground motion and three-dimensional amplification effects in the Taipei basin by using a composite grid finite-difference method, *Bull. Seismol. Soc. Am.,* **98**(3), 1229–1242.

Lee, S.J., Chen, H.W. Liu, Q., Komatitsch, D., Huang, B.S. & Tromp, J., 2008b. Mesh generation and strong motion simulations in the Taipei basin based upon the spectral-element method, *Bull. Seismol. Soc. Am.,* **98**(1), 253–264, doi:10.1785/0120070033.

Lee, S.J., Chen, H.W. & Ma, K.F., 2007. Strong motion simulation of the 1999, Chi-Chi, Taiwan earthquake from a realistic three-dimensional source and crustal structure, *J. Geophys. Res.,* **112,** B06307, doi:10.1029/2006JB004615.

Lin, C.H., 2000. Thermal modeling of continental subduction and exhumation constrained by heat flow and seismicity in Taiwan, *Tectonophysics,* **324,** 189–201.

Lin, C.H. & Ando, M., 2004. Seismological evidence of simultaneous mountain-building and crust-thickening from the 1999 Taiwan Chi-Chi earthquake (Mw = 7.6), *Earth Planets Space,* **56**, 163–167.

Lin, C.H., 2005. Identification of mantle reflections from a dense linear seismic array: Tectonic implications to the Taiwan orogeny, *Geophys. Res. Lett.,* **32,** L06315, doi:10.1029/2004GL021814.

Ligorría J.P. & Ammon, C.J., 1999. Iterative deconvolution and receiver-function estimation, *Bull. Seismol. Soc. Am.,* **89**(5), 1395–1400.

Mori, J. & Helmberger, D., 1996. Large-amplitude Moho reflections (SmS) from Landers aftershocks, southern California, *Bull. Seismol. Soc. Am.,* **86**(6), 1845–1852.

Niu, F., Levander, A., Ham, S. & Obayashi, M., 2005. Mapping the subducting Pacific slab beneath southwest Japan with Hi-net receiver functions, *Earth and Planetary Sci. Lett.,* **239,** 9–17.

Owens, T.J., Crotwell, H.P., Groves, C. & Oliver-Paul, P., 2004. SOD: Standing Order for Data, *Seismological Research Lett.,* **75,** 515–520.

Rau, R.J. & Wu, F.T., 1995. Tomographic imaging of lithospheric structures under Taiwan, *Earth planet. Sci. Lett.,* **133,** 517–532.

Shih, R.C., Lin, C.H., Lai, H.L., Yeh, Y.H, Huang, B.S. & Yen, H.Y., 1998. Preliminary crustal structures across Central Taiwan from modeling of the onshore-offshore wide-angle seismic data, *Terr. Atm. Ocean.,* **9**(3), 317–328.

Suppe, J., 1987. *The active Taiwan mountain belt, in The Anatomy of Mountain Ranges,* pp. 277–293, eds Schaer, J.P. & Rogers, J., Princeton Univ. Press, New Jersey.

Tapponnier, P., Xu, Z., Francoise, R., Bertrand, M., Nicolas, A., W. Gerard, W. & Yang, J., 2001. Oblique stepwise rise and growth of the Tibet Plateau, *Science,* 23, **294**(5547), 1671–1677.

Tomfohrde, D.A. & Nowack, R.L., 2000. Crustal structure beneath Taiwan using frequency-band inversion of receiver function waveforms, *Pure and Appl. Geophys.,* **157,** 737–764.

Wu, F.T., Rau, R.J. & Salzberg, D., 1997. Taiwan orogengy: think-skinned or lithospheric collision? *Tectonophysics,* **274,** 191–220.

Wu, Y.M., Chang, C.H., Zhao, L., Shyu, J.B.H., Chen, Y.-G., Sieh, K. & Avouac, J.P., 2007, Seismic tomography of Taiwan: Improved constraints from a dense network of strong motion stations, *J. Geophys. Res.,* **112,** B08312, doi:10.1029/2007JB004983.

Wu, Y.M., Chang, C.H., Zhao, L., Teng, T.L. & Nakamura, M., 2008. A comprehensive relocation of earthquakes in Taiwan from 1991 to 2005, *Bull. seism. Soc. Am.,* **98**(3), 1471–1481, doi:10.1785/0120070166.

Yamauchi, M., Hirahara, K. & Shibutani, T., 2003. High resolution receiver function imaging of the seismic velocity discontinuities in the crust and uppermost mantle beneath southwest Japan, *Earth Planets Space,* **55,** 59–64.

Yeh, Y.H., Shih, R.C., Lin, C.H, Liu, C.C., Yen, H.Y., Huang, B.S., Liu, C.S. & Wu, F.T., 1998. Onshore/offshore wide-angle deep seismic profiling in Taiwan, *Terr. Atm. Ocean.,* **9**(3), 301–316.

Yen, H.Y., Yeh, Y.H. & Wu, F.T., 1998. Two-dimensional crustal structures of Taiwan from gravity data, *Tectonics,* **17**(1), 104–111.

Yu, S.B., Chen, H.Y. & Kuo, L.C., 1997. Velocity field of GPS stations in the Taiwan area, *Tectonophysics,* **274,** 41–59.

Yu, Y. E., 2008. *Seismic travel-time studies on reference models evaluation, earthquake location and crustal structure in west central Taiwan,* Master thesis, National Central University.

Zandt, G. & Ammon, C.J., 1995. Continental crust composition constrained by measurements of crustal Poisson's ratio, *Nature,* **374,** 152–154.

Zandt, G., Myers, S.C. & Wallace, T. C., 1995. Crust and mantle structure across the Basin and Range-Colorado Plateau boundary at 37°N latitude and implications for Cenozoic extensional mechanism, *J. Geophys. Res.,* **100,** 10529–10548.

Zhu, L., 2000. Crustal structure across the San Andreas Fault, southern California from teleseismic converted waves, *Earth planet. Sci. Lett.,* **279,** 183–190.

Zhu, L., Zeng, R.S., Wu, F.T., Owens, T.J. & Randall, G.E., 1993. Preliminary study of of the Tibetan plateau by using broadband teleseismic body waveforms, *Acta Seismologica Sinica,* **6,** 305–316.

Zhu, L., Owens, T.J. & Randall, G.E., 1995. Lateral variation in crustal structure of the northern Tibetan plateau inferred from teleseismic receiver functions, *Bull. Seismol. Soc. Am.,* **85**(6), 1531–1540.

Zhu, L. & Kanamori, H., 2000. Moho depth variation in southern California from teleseismic receiver function, *J. Geophys. Res.,* **105,** 2969–1980.

Zhu, L., Mitchell, B.J., Akyol, N., Cemen, I. & Kekovali, K., 2006. Crustal thickness variations in the Aegean region and implications for the extension of continental crust, *J. Geophys. Res.,* **111,** B01301, doi:10.1029/2005JB003770.

SUPPORTING INFORMATION

Additional Supporting Information may be found in the online version of this article:

The attached video files show the 3-D perspective view of earthquake seismicity and the proposed Taiwan Reference Moho Discontinuity Models (TRMDMs) constraints by stations in central Taiwan. The supplementary video files are all in gif format. Videos S1 and S2 show the variation of Moho topography changes derived from piecewise bicubic spline interpolation among all BATS stations in Taiwan.

Video S1: The zoom-in view to show the large depth variation indicated in Fig. 8(a) mainly caused by the deepest Moho depth at station SSLB.

Video S2: The alternative solution of TRMDM, which shows a more pronounced Moho topography change across stations between TDCB and SSLB in Fig. 8(b). The geometry of the Moho surface may be subject to change, however, such a large-scale feature ought to be the same.

Please note: Wiley-Blackwell are not responsible for the content or functionality of any supporting materials supplied by the authors. Any queries (other than missing material) should be directed to the corresponding author for the article.